

4 **Impact of jet production data on the next-to-next-to-leading order**
5 **determination of HERAPDF2.0 parton distributions**

6 **Paper Draft v1.6 – October 11, 2021**
7 **Reading**

8 Author list

9 **Abstract**

10 The HERAPDF2.0 ensemble of parton distribution functions (PDFs) was introduced in
11 2015. Presented is the final stage, a next-to-next-to-leading order (NNLO) analysis of the
12 HERA data on inclusive deep inelastic ep scattering together with jet data as published by
13 the H1 and ZEUS collaborations. A pQCD fit of $\alpha_s(M_Z^2)$ together with the PDFs to the data
14 was used to determine $\alpha_s(M_Z^2)$ with the result $\alpha_s(M_Z^2) = 0.1156 \pm 0.0011$ (exp^{+0.0001}_{-0.0002} (model
15 +parameterisation) ± 0.0029 (scale). The PDF sets of HERAPDF2.0Jets NNLO were de-
16 termined with fits using the fixed values of $\alpha_s(M_Z^2) = 0.1155$ and $\alpha_s(M_Z^2) = 0.118$. The
17 latter value was already chosen for the published HERAPDF2.0 NNLO analysis based on
18 inclusive data only. The different sets of PDFs are presented, evaluated and compared. The
19 consistency of the PDFs demonstrates the consistency of HERA inclusive and jet-production
20 cross-section data. Predictions based on HERAPDF2.0Jets NNLO agree within uncertain-
21 ties with the measured jet-production cross sections used as input to the fits.

22 *To be submitted to EPJC*

1 Introduction

Data from deep inelastic scattering (DIS) of electrons¹ on protons, ep , at centre-of-mass energies of up to $\sqrt{s} \approx 320$ GeV recorded at HERA, have been central to the exploration of proton structure and quark–gluon dynamics as described by perturbative Quantum Chromo Dynamics (pQCD) [1].

The combination of H1 and ZEUS data on inclusive ep scattering and the subsequent pQCD analysis, introducing the ensemble of parton density functions (PDFs) known as HERAPDF2.0, were milestones in the exploitation [2] of the HERA data. These analyses are based on pQCD fits to the HERA DIS data in the DGLAP [3–7] formalism using the $\overline{\text{MS}}$ scheme [8].

The sets of PDFs presented in this work complete the HERAPDF2.0 ensemble [2] of PDFs. They were determined with a next-to-next-leading order (NNLO) analysis of HERA inclusive DIS data [2] and selected jet-production data as published separately by the H1 and ZEUS collaborations [9–14]. An analysis of jet data at NNLO was not possible at the time of the introduction of the HERAPDF2.0 ensemble. It has become possible by the recent provision of jet cross-section predictions for ep scattering at NNLO [15–23].

The strategy chosen for the analysis presented here follows that of the previous HERA-PDF2.0 Jets NLO analysis [2]. Jet cross section data are included in the pQCD analysis to constrain the gluon PDF which, however, is correlated with the value of the strong coupling, $\alpha_s(M_Z^2)$. Thus, the PDFs and the value of $\alpha_s(M_Z^2)$ were fit simultaneously, and then the resulting $\alpha_s(M_Z^2)$ was used to refit the PDFs with $\alpha_s(M_Z^2)$ fixed to this value in order to determine the uncorrelated uncertainties at this value of $\alpha_s(M_Z^2)$. The PDFs were also determined for $\alpha_s(M_Z^2) = 0.118$, the PDG18 value [24].

The calculation of jet cross-sections at NNLO is based on jets starting from massless partons. The inclusive data, on the other hand, are treated within the RTOPT [25–27] Variable Flavour Number Scheme (VFNS), which requires values of the parameters for the charm- and beauty-quark masses, M_c and M_b , as input. These parameters were optimised via QCD fits using both the inclusive data and the cross sections for charm and beauty production that were published as combined data by the H1 and ZEUS collaborations [28]. However, the heavy-quark data were not explicitly included in the pQCD fits that included jet data because of the different treatment of the mass parameters in the two data sets.

The results presented here are based entirely on HERA data, i.e. inclusive DIS and jet-production data. The HERA inclusive data are a single, consistent data set, taking all systematic uncertainties into account. Furthermore, the jet data have been found to be consistent with the inclusive data at NLO [2]; the analysis presented here also tests their consistency at NNLO. In addition, PDF fits to LHC data might be biased by any physics Beyond the Standard Model (BSM) whose effects have so far escaped detection, thereby reducing the sensitivity of searches for BSM due to biased background predictions. Thus, the HERAPDF2.0 ensemble of PDFs provides a benchmark to which PDFs including data from LHC colliders may be compared. This could reveal BSM effects or the need for an extension of the QCD analyses for some processes.

¹From here on, the word “electron” refers to both electrons and positrons, unless otherwise stated.

2 Data

Data taken by the H1 and ZEUS collaborations from 1993 to 2007 were combined to form a consistent set of inclusive HERA ep DIS cross sections [2] taking all systematic uncertainties into account in a coherent way. This set of data was used as input to the determinations of all previous members of the HERAPDF2.0 ensemble. The HERAPDF2.0Jets analysis at NLO, in addition, used selected data [9–12,14] on inclusive jet and dijet production from H1 and ZEUS, which were again used for the present analysis at NNLO. In addition, new data published by the H1 collaboration on jet production [13,14] were added as input to the NNLO analysis. These are data on events at lower Q^2 , where Q^2 is the four-momentum-transfer in the DIS process squared, together with six new high- Q^2 points at low p_T , where p_T is the transverse momentum of the jet.

A summary on the data of jet production used is provided in Table 1. For all data sets, the jets were identified with the k_T algorithm with the R parameter set to one.

The predictions on inclusive jet and dijet production at NNLO were only applicable to a slightly reduced phase space compared to HERAPDF2.0Jets NLO. All data points with $\mu = \sqrt{\langle p_T^2 \rangle + Q^2} \leq 10.0 \text{ GeV}$ had to be excluded in order to ensure the convergence of the perturbative series and to limit the NNLO scale uncertainties of the theoretical predictions to below 10% compared to below 24% at NLO. This requirement on μ also ensured that μ was larger than the b -quark mass, which is necessary because the jets are built from massless partons in the calculation of the NNLO predictions. In addition, for each Q^2 interval, the six data points with the lowest $\langle p_T \rangle$ were excluded from the ZEUS dijet data set because the available NNLO predictions for these points were incomplete when considering the kinematic cuts². The resulting reduction of data points is detailed in Table 1. In addition, the trijet data [14] which were used as input to HERAPDF2.0Jets NLO were excluded as no NNLO treatment was available.

The inclusive charm data [29], which were included in the analysis at NLO [2], were not explicitly used in the PDF fits of the analysis presented here, since complete NNLO predictions were not available. Heavy quark data [28] were only used to optimise the mass parameter values for charm, M_c , and beauty, M_b , which are needed as input to the adopted RTOPT [27] NNLO approach to the fitting of the inclusive data.

3 QCD analysis

The present analysis was performed in the same way as all previous HERAPDF2.0 analyses [2]. Only cross sections for $Q^2 \geq Q_{\min}^2$ with $Q_{\min}^2 = 3.5 \text{ GeV}^2$ were used in the analysis. The χ^2 definition was taken from equation (32) of the previous paper [2]. The value of the starting scale for the DGLAP evolution was taken as $\mu_{f0}^2 = 1.9 \text{ GeV}^2$. The parameterisation of the PDFs and the choice of free parameters also followed the prescription for the HERAPDF2.0Jets NLO analysis, see Section 3.1.

All fits were performed using the programme QCDNUM [30] within the xFitter (formerly HERAFitter) framework [31] and were cross-checked with an independent programme, which

²Due to the kinematic cuts used in selecting the dijet data, the LO prediction for the cross sections is zero. Thus, the NNLO term is only the second non-zero term.

99 was already used for cross-checks in the HERAPDF2.0 analysis. The results obtained using the
 100 two programmes, as previously for all HERAPDF2.0 fits [2], were in excellent agreement, i.e.
 101 well within fit uncertainties. All numbers presented here were obtained using xFitter.

102 The light-quark coefficient functions were calculated in QCDNUM. The heavy-quark coeffi-
 103 cient functions were calculated in the general-mass variable-flavour-number scheme RTOPT [25],
 104 with recent modifications [26,27], see Section 3.3

105 The analysis presented here was made possible by the newly available treatment of jet pro-
 106 duction at NNLO [15–23] using the zero-mass scheme. This is expected to be a reasonable ap-
 107 proximation when the relevant QCD scales are significantly above the charm- and beauty-quark
 108 masses. The jet data were included in the fits at full NNLO using predictions for the jet cross
 109 sections calculated using NNLOJET [15–17], which was interfaced to the fast interpolation grid
 110 codes, fastNLO [18–20] and APPLgrid [21,22] using the APPLfast framework [23], in order
 111 to achieve the required speed for the convolutions needed in an iterative PDF fit. The NNLO
 112 jet predictions were provided in the massless scheme and were corrected for hadronisation and
 113 Z^0 exchange before they were used in the fits. A running electromagnetic α as implemented in
 114 the 2012 version of the programme EPRC [32] was used in the treatment of the jet cross sec-
 115 tions. The predictions included uncertainties, which were taken into account in all fits as 50 %
 116 correlated and 50 % uncorrelated between processes and bins.

117 The choice of scales for the jet data had to be adjusted for the NNLO analysis. At NLO, the
 118 factorisation scale was chosen as for the inclusive data, i.e. $\mu_f^2 = Q^2$, while the renormalisation
 119 scale was linked to the transverse momenta, p_T , of the jets as $\mu_r^2 = (Q^2 + p_T^2)/2$. For the NNLO
 120 analysis, $\mu_f^2 = \mu_r^2 = Q^2 + p_T^2$ was used. This has resulted in an improved χ^2 for the fits, confirming
 121 previously published studies [37]. Scale variations were also considered and are discussed in
 122 Sections 4.1 and 4.2. In general, scale variations are used to estimate the uncertainties due to
 123 missing higher order contributions.

124 3.1 Choice of PDF parameterisation and model parameters

125 The choice of parameterisation follows the original concept of HERAPDF2.0, for which all
 126 details were previously published [2]. The parameterisation is an effective way to store the
 127 information derived from many data points in a limited set of numbers. The parameterised
 128 PDFs, $x f(x)$, are the gluon distribution xg , the valence-quark distributions xu_v , xd_v , and the u -
 129 type and d -type anti-quark distributions $x\bar{U}$, $x\bar{D}$, where $x\bar{U} = x\bar{u}$ and $x\bar{D} = x\bar{d} + x\bar{s}$ at the chosen
 130 starting scale. The generic form of the parameterisation for a PDF $f(x)$ is

$$131 \quad x f(x) = A x^B (1-x)^C (1 + D x + E x^2). \quad (1)$$

132 For the gluon PDF, an additional term of the form $A'_g x^{B'_g} (1-x)^{C'_g}$ is subtracted³.

133 Not all the D and E parameters were actually used in the fit. The so-called χ^2 saturation
 134 method [2,33] was used to select the parameters used. Initially all D and E parameters as well

³The parameter $C'_g = 25$ was fixed since the fit is not sensitive to this value, provided it is high enough ($C'_g > 15$) ensuring that the term does not contribute at large x .

135 as A'_g were set to zero. Extra parameters were introduced one at a time until the χ^2 of the fit
 136 could not be further improved. This resulted in a final parameterisation

$$137 \quad xg(x) = A_g x^{B_g} (1-x)^{C_g} - A'_g x^{B'_g} (1-x)^{C'_g}, \quad (2)$$

$$138 \quad xu_v(x) = A_{u_v} x^{B_{u_v}} (1-x)^{C_{u_v}} (1 + E_{u_v} x^2), \quad (3)$$

$$139 \quad xd_v(x) = A_{d_v} x^{B_{d_v}} (1-x)^{C_{d_v}}, \quad (4)$$

$$140 \quad x\bar{U}(x) = A_{\bar{U}} x^{B_{\bar{U}}} (1-x)^{C_{\bar{U}}} (1 + D_{\bar{U}} x), \quad (5)$$

$$141 \quad x\bar{D}(x) = A_{\bar{D}} x^{B_{\bar{D}}} (1-x)^{C_{\bar{D}}}. \quad (6)$$

142 The normalisation parameters, A_g, A_{u_v}, A_{d_v} , were constrained by the quark-number and momen-
 143 tum sum rules. The B parameters, $B_{\bar{U}}$ and $B_{\bar{D}}$, were set equal, $B_{\bar{U}} = B_{\bar{D}}$, resulting in a single B
 144 parameter for the sea distributions.

145 The strange-quark distribution was expressed as an x -independent fraction, f_s , of the d -type
 146 sea, $x\bar{s} = f_s x\bar{D}$ at Q_0^2 . The central value $f_s = 0.4$ was chosen to be a compromise between the
 147 determination of a suppressed strange sea from neutrino-induced di-muon production [34,35]
 148 and the determination of an unsuppressed strange sea from the ATLAS collaboration [36]. The
 149 further constraint $A_{\bar{U}} = A_{\bar{D}}(1-f_s)$, together with the requirement $B_{\bar{U}} = B_{\bar{D}}$, ensured that $x\bar{u} \rightarrow x\bar{d}$
 150 as $x \rightarrow 0$.

151 The final parameterisation together with the constraints became the basis of the 14 parameter
 152 fit which was used throughout the analysis. The parameterisation is identical to the parameter-
 153 isation used previously for the inclusive data. The jet data did not require extra parameters. The
 154 fit satisfies the criteria that all PDFs and all predicted cross sections are positive throughout the
 155 kinematic region probed by the data entering the fit.

156 3.2 Model and parameterisation uncertainties

157 Model and parameterisation uncertainties on the PDFs determined by a central fit were evaluated
 158 with fits with modified input assumptions. The central values of the model parameters and their
 159 variations are summarised in Table 2. The uncertainties on the PDFs obtained from variations
 160 of $M_c, M_b, f_s, Q_{\min}^2$ were added in quadrature, separately for positive and negative uncertainties,
 161 and represent the model uncertainty.

162 The symmetrised uncertainty obtained from the downward variation of $\mu_{f_0}^2$ from 1.9 GeV
 163 to 1.6 GeV, see also Section 3.3, was taken as a parameterisation uncertainty. In addition, a
 164 variation of the number of terms in the polynomial $(1 + Dx + Ex^2)$ was considered for each of the
 165 parton distributions listed in Eqs. (2) – (6). For this, all 15-parameter fits which have one more
 166 non-zero free D or E parameter were considered as possible variants and the resulting PDFs
 167 compared to the PDF from the 14-parameter central fit. The only significant change in the PDFs
 168 was observed for the addition of a D_{u_v} parameter. The uncertainties on the central fits from the
 169 parameterisation variations were stored as an envelope representing the maximal deviation at
 170 each x value.

171 The total uncertainties on the PDFs were obtained by adding experimental, i.e. fit, model
 172 and parameterisation uncertainties in quadrature.

173 3.3 Optimisation of M_c and M_b

174 The RTOPT scheme used to calculate predictions for the inclusive data requires the charm- and
 175 beauty-mass parameters, M_c and M_b , as input. The optimal values of these parameters were
 176 reevaluated using the standard procedure [2,33], applied to the new combined HERA data on
 177 heavy quarks [28] together with the combined inclusive data [2]. The procedure comprises
 178 multiple pQCD fits with varying choices of the M_c and M_b parameters. The parameter values
 179 resulting in the lowest χ^2 values of the fit were chosen. This was done both at NNLO and NLO
 180 to provide consistent sets of M_c and M_b for future pQCD analyses. The one standard-deviation
 181 uncertainties of the mass parameters were determined by fitting the χ^2 values with a quadratic
 182 function and finding the mass-parameter values corresponding to $\Delta\chi^2 = 1$.

183 At NNLO (NLO), the fits for the optimisation were performed with fixed values of $\alpha_s =$
 184 0.1155^4 ($\alpha_s = 0.118$)⁵. As a first iteration at NNLO (NLO), M_c was varied with fixed $M_b =$
 185 4.5 GeV (4.5 GeV) and M_b was varied with fixed $M_c = 1.43 \text{ GeV}$ (1.47 GeV), i.e. the mass-
 186 parameter values used for HERAPDF2.0 NNLO (NLO) were used as fixed points. In every
 187 iteration to determine M_b (M_c), the mass-parameter value for M_c (M_b) as obtained from the
 188 previous iteration was used as a new fixed point. The iterations were ended once values stable
 189 within 0.1 % for M_c and M_b were observed. The final χ^2 scans at NNLO are shown in Figs. 1 a)
 190 and 1 c) and at NLO in Figs. 1 b) and 1 d). The resulting values at NNLO are $M_c = 1.41 \pm$
 191 0.04 GeV and $M_b = 4.20 \pm 0.10 \text{ GeV}$, quite close to the values determined for HERAPDF2.0
 192 NNLO, with slightly reduced uncertainties. The values at NLO are $M_c = 1.46 \pm 0.04 \text{ GeV}$ and
 193 $M_b = 4.30 \pm 0.10 \text{ GeV}$. The minimum in χ^2 for the parameter M_c at NNLO is observed close to
 194 the technical limit of the fitting procedure.

195 The part of the model uncertainty concerning the heavy-flavour mass parameters would nom-
 196 inally have involved varying the value of M_c to the minimum and maximum of its one standard-
 197 deviation uncertainty. However, for M_c , the downward variation created a conflict with μ_{f0} ,
 198 which has to be less than M_c in the RTOPT scheme, such that charm can be generated pertur-
 199 batively. Thus, only an upward variation of M_c was considered and the resulting uncertainty on
 200 the PDFs was symmetrised. In addition, the requirement of $\mu_{f0} < M_c$ created a conflict with
 201 the variation of μ_{f0}^2 . The normal procedure would have included an upward variation of μ_{f0}^2
 202 to 2.2 GeV^2 but μ_{f0} would have become larger than the upper end of the uncertainty interval of M_c ⁶.
 203 Thus, μ_{f0}^2 was only varied downwards to 1.6 GeV^2 , and the resulting uncertainty on the PDFs
 204 was again symmetrised. The suitability of the chosen central parameterisation was re-verified
 205 for the new settings for M_c and M_b using the χ^2 saturation method as described in Section 3.1.

206 Since predictions at NNLO for the jet data were only available in the zero-mass scheme,
 207 and results for the treatment of the inclusive data in different VFNS and FFNS schemes were
 208 consistent [2], no other heavy-flavour schemes were investigated.

209 3.4 Hadronisation uncertainties

210 For the jet-data analysis, it was also necessary to consider hadronisation and the effect of the
 211 uncertainties on hadronisation corrections. The uncertainties on the hadronisation corrections,

⁴A cross-check was performed with the fixed value of $\alpha_s = 0.118$ and no significant difference in the resulting M_c and M_b values were observed.

⁵The value 0.118 was used in the pQCD analysis of heavy quark data [28].

⁶In previous HERAPDF analyses, the uncertainty on M_c was large enough to accommodate the upward μ_{f0}^2 variation.

212 which were supplied in the original publications, were reviewed for this analysis. The H1 un-
 213 certainties were used as published, while for technical reasons, those for the ZEUS data were
 214 increased to the maximum value quoted in the publications, 2 %. This change resulted in no
 215 significant difference to any of the results presented here.

216 In the HERAPDF2.0Jets NLO analysis, hadronisation uncertainties were applied using the
 217 offset method, i.e. performing separate fits with the hadronisation corrections set to their maxi-
 218 mal and minimal values. This resulted in a hadronisation uncertainty on $\alpha_s(M_Z^2)$ of ± 0.0012 [2].

219 The current procedure differs from that used previously. The uncertainties on the hadronisa-
 220 tion corrections were included as input to the HERAPDF2.0 Jets NNLO fits. They were treated
 221 as systematic uncertainties, 50 % correlated and 50 % uncorrelated between bins and data sets.
 222 Thus, their contribution became part of the overall experimental, i.e. fit, uncertainties. For fits
 223 with fixed $\alpha_s(M_Z^2)$, their contribution was negligible. For fits with free $\alpha_s(M_Z^2)$, their contribution
 224 to the experimental uncertainty on $\alpha_s(M_Z^2)$ was ± 0.0006 . This represents a significant reduction
 225 of the influence of the hadronisation uncertainties compared to previous analyses.

226 4 HERAPDF2.0Jets NNLO – results

227 4.1 Simultaneous determination of $\alpha_s(M_Z^2)$ and PDFs

228 Jet-production data are essential for the determination of the strong coupling constant, $\alpha_s(M_Z^2)$.
 229 Inclusive DIS is dominated by a QED vertex and, thus, in pQCD fits to inclusive DIS data
 230 alone, the gluon PDF is only determined via the DGLAP equations, using the observed scaling
 231 violations. This results in a strong correlation between the shape of the gluon distribution and
 232 the value of $\alpha_s(M_Z^2)$. Data on jet and dijet production cross-sections provide an independent
 233 constraint on the gluon distribution and are also directly sensitive to $\alpha_s(M_Z^2)$. Thus, such data are
 234 essential for an accurate simultaneous determination of $\alpha_s(M_Z^2)$ and the gluon distribution.

235 When determining $\alpha_s(M_Z^2)$, it is necessary to consider so-called “scale uncertainties”, which
 236 serve as an approximate proxy for the uncertainties due to the unknown influence of higher
 237 orders in the perturbation expansion. These uncertainties were evaluated by varying the renor-
 238 malisation and factorisation scales by a factor of two, both separately and simultaneously⁷, and
 239 selecting the maximal positive and negative deviations of the result as the “de facto” scale un-
 240 certainties. These were observed for $(2.0\mu_r, 1.0\mu_f)$ and $(0.5\mu_r, 1.0\mu_f)$, respectively.

241 The HERAPDF2.0Jets NNLO fit with free $\alpha_s(M_Z^2)$ results in

$$242 \quad \alpha_s(M_Z^2) = 0.1156 \pm 0.0011 \text{ (exp)} \quad {}_{-0.0002}^{+0.0001} \text{ (model + parameterisation)} \pm 0.0029 \text{ (scale)} \quad , \quad (7)$$

243 where “exp” denotes the experimental uncertainty, which was taken as the fit uncertainty, includ-
 244 ing the contribution from hadronisation uncertainties. The value of $\alpha_s(M_Z^2)$ and the size of the
 245 experimental uncertainty were confirmed by the result of a scan in $\alpha_s(M_Z^2)$, for which the result-
 246 ing χ^2 values are shown in Fig. 2 a). The clear minimum observed in χ^2 coincides with the value
 247 of $\alpha_s(M_Z^2)$ listed in Eq. (7). The width of the minimum in χ^2 confirms the fit uncertainty. The

⁷This procedure is often called 9-point variation, where the nine variations are $(0.5\mu_r, 0.5\mu_f)$, $(0.5\mu_r, 1.0\mu_f)$,
 $(0.5\mu_r, 2.0\mu_f)$, $(1.0\mu_r, 0.5\mu_f)$, $(1.0\mu_r, 1.0\mu_f)$, $(1.0\mu_r, 2.0\mu_f)$, $(2.0\mu_r, 0.5\mu_f)$, $(2.0\mu_r, 1.0\mu_f)$, $(2.0\mu_r, 2.0\mu_f)$.

248 combined model and parameterisation uncertainty shown in Fig. 2 a) was determined by per-
 249 forming similar scans, for which the values of the model parameters and the parameterisation
 250 were varied as described in Section 3.1.

251 Figure 2 a) also shows the scale uncertainty, which dominates the total uncertainty. The
 252 scale uncertainty as listed in Eq. (7) was evaluated under the assumption of 100 % correlated
 253 uncertainties between bins and data sets. The previously published result at NLO [2] had scale
 254 uncertainties calculated under the assumption of 50 % correlated and 50 % uncorrelated uncer-
 255 tainties between bins and data sets. A strong motivation to determine $\alpha_s(M_Z^2)$ at NNLO was the
 256 hope of a substantial reduction in the scale uncertainty. Therefore, the analysis was repeated
 257 for these assumptions in order to be able to compare the NNLO to the NLO scale uncertainties.
 258 The reevaluated NNLO scale uncertainty of (± 0.0022) is indeed significantly lower than the
 259 ($+0.0037, -0.0030$) previously observed in the HERAPDF2.0Jets NLO analysis.

260 The HERAPDF2.0Jets NNLO fit with free $\alpha_s(M_Z^2)$ was based on 1363 data points and had
 261 a $\chi^2/\text{degree of freedom(d.o.f.)} = 1614/1348 = 1.197$. This can be compared to the $\chi^2/\text{d.o.f.} =$
 262 $1363/1131 = 1.205$ for HERAPDF2.0 NNLO based on inclusive data only [2]. The similarity
 263 of the $\chi^2/\text{d.o.f.}$ values indicates that the data on jet production do not introduce any additional
 264 tension to the fit. The jet data are fully consistent with the inclusive data.

265 The question of whether data at relatively low Q^2 bias the determination of $\alpha_s(M_Z^2)$ arose
 266 within the context of the HERAPDF2.0 analysis [2]. Figure 2 b) shows the result of $\alpha_s(M_Z^2)$
 267 scans with Q_{\min}^2 for the inclusive data set to 3.5 GeV^2 , 10 GeV^2 and 20 GeV^2 . The positions of
 268 the minima are in good agreement, indicating that any anomalies at low Q^2 are small. Figure 2 c)
 269 shows the result of similar scans with only the inclusive data used as input [2]. The inclusive
 270 data alone cannot sufficiently constrain $\alpha_s(M_Z^2)$.

271 To verify that the use of the A'_g term in the gluon parameterisation does not bias the determi-
 272 nation of $\alpha_s(M_Z^2)$, cross-checks were made with two modified gluon parameterisations. These are
 273 $A'_g = 0$ and $xg(x) = A_g x^{B_g} (1-x)^{C_g}$ as well as the alternative gluon parameterisation, AG [2], for
 274 which $A'_g = 0$ and $xg(x) = A_g x^{B_g} (1-x)^{C_g} (1 + D_g x)$. A value of $\alpha_s(M_Z^2) = 0.1151 \pm 0.0010$ (exp)
 275 was obtained for both modifications of the parameterisation, which is in agreement with the
 276 result for the standard parameterisation. The value of D_g in the AG parameterisation was con-
 277 sistent with zero. These results demonstrate that the present $\alpha_s(M_Z^2)$ determination is not very
 278 sensitive to the details of the gluon parameterisation.

279 Other determinations of $\alpha_s(M_Z^2)$ at NNLO using jet data as published by H1 [37] and NNLO-
 280 JET authors and their collaborators [38] used fixed PDFs for their fits to determine $\alpha_s(M_Z^2)$.
 281 While this is a common procedure, it could bias the resulting value of $\alpha_s(M_Z^2)$ [39]. Thus, the
 282 values of $\alpha_s(M_Z^2)$ should not be directly compared. However, both analyses were performed with
 283 a cut on μ of $\mu > 2M_b$, which is quite similar to the $\mu > 10.0 \text{ GeV}$ cut used for this analysis.
 284 Thus, the scale uncertainties can be compared. The H1 result is based on H1 data only and
 285 the quoted scale uncertainty is ± 0.0039 . The scale uncertainty published by NNLOjet using
 286 H1 and ZEUS data ± 0.0033 . This can be compared to the ± 0.0029 obtained for the analysis
 287 presented here. The somewhat reduced scale uncertainty for the present analysis could be due
 288 to the correlation between PDFs and $\alpha_s(M_Z^2)$ such that the evolution of the fixed PDFs increase
 289 the dependence of $\alpha_s(M_Z^2)$ on the chosen scales.

290 The H1 collaboration provided one simultaneous fit of $\alpha_s(M_Z^2)$ and PDFs using a ZMVFN
 291 scheme [37]. It was based on H1 inclusive and jet data with $Q_{\min}^2 = 10 \text{ GeV}^2$. For comparison,

292 the analysis presented here was modified by also setting $Q_{\min}^2 = 10 \text{ GeV}^2$. The value of $\alpha_s(M_Z^2)$
 293 published by H1 is $\alpha_s(M_Z^2) = 0.1147 \pm 0.0011$ (exp) ± 0.0002 (model) ± 0.0003 (parameterisation) \pm
 294 0.0023 (scale) while the current modified analysis resulted in $\alpha_s(M_Z^2) = 0.1156 \pm 0.0011$ (exp) \pm
 295 0.0002 (model + parameterisation) ± 0.0021 (scale). These values agree within uncertainties.
 296 Overall, the various determinations of $\alpha_s(M_Z^2)$ provide a very consistent picture up to NNLO.

297 4.2 The PDFs of HERAPDF2.0Jets NNLO obtained for fixed $\alpha_s(M_Z^2)$

298 The values of $\alpha_s(M_Z^2) = 0.1155$ and $\alpha_s(M_Z^2) = 0.118$ were used for the determination of the
 299 two sets of PDFs released from HERAPDF2.0Jets NNLO analysis, see Appendix A. The value
 300 of $\alpha_s(M_Z^2) = 0.1155$ corresponds to the determination of $\alpha_s(M_Z^2)$ presented in Section 4.1. The
 301 value of $\alpha_s(M_Z^2) = 0.118$ was the result of the HERAPDF2.0Jets NLO analysis and was used
 302 for the HERAPDF2.0 analyses at NNLO based on inclusive data only [2]. The PDFs of HERA-
 303 PDF2.0Jets NNLO are shown in Fig. 3 a) and b) for both, fixed $\alpha_s(M_Z^2) = 0.1155$ and fixed
 304 $\alpha_s(M_Z^2) = 0.118$, respectively, together with their uncertainties, at the scale $\mu_f^2 = 10 \text{ GeV}^2$. The
 305 uncertainties shown are the experimental, i.e. fit, uncertainties as well as the model and parame-
 306 terisation uncertainties as defined in Section 3.2. The parameterisation uncertainty dominates
 307 the uncertainties and is itself dominated by the introduction of the parameter D_{u_v} as a variation.

308 As the PDFs were derived with fixed $\alpha_s(M_Z^2)$ values, uncertainties on the PDFs from varying
 309 the scales in the fit procedure were not considered, because, in this case, a quantification of
 310 the influence of higher orders by varying the renormalisation and factorisation scales in the
 311 fit becomes questionable. Any variation of the renormalisation scale effectively amounts, in
 312 its numerical effect, to a modification of the value of $\alpha_s(M_Z^2)$, since the compensation with the
 313 explicit scale-dependent terms in the NLO and NNLO coefficients is incomplete. If a fit is
 314 performed with a fixed value of $\alpha_s(M_Z^2)$, it might thus not reach a local minimum. However, such
 315 a local minimum is required to estimate the unknown amount of influence of higher orders by
 316 varying the scales. Nevertheless, a cross-check with scale variations as described in Section 4.1
 317 was made. The impact on the resulting PDFs was found to be negligible compared to the other
 318 uncertainties presented in Fig. 3.

319 A comparison between the PDFs obtained for $\alpha_s(M_Z^2) = 0.1155$ and $\alpha_s(M_Z^2) = 0.118$ is
 320 provided in Figs. 4 and 5 for the scales $\mu_f = 10 \text{ GeV}^2$ and $\mu_f = M_Z^2$, respectively. Here, only
 321 total uncertainties are shown. At the lower scale, a significant difference is observed between
 322 the gluon PDFs; the PDF for $\alpha_s(M_Z^2) = 0.1155$ is above the PDF for $\alpha_s(M_Z^2) = 0.118$ for x less
 323 than $\approx 10^{-2}$. This correlation between the value of $\alpha_s(M_Z^2)$ and the shape of the gluon PDF is
 324 as expected from QCD evolution. At the scale of M_Z^2 , the differences become negligible in the
 325 visible range of x due to QCD evolution.

326 A comparison of the PDFs obtained for $\alpha_s(M_Z^2) = 0.118$ by HERAPDF2.0Jets NNLO to the
 327 PDFs of HERAPDF2.0 NNLO, based on inclusive data only, is provided in Fig. 6. These two
 328 sets of PDFs do not show any significant difference in the central values. However, there is a
 329 significant reduction of the uncertainties on the gluon PDFs from the HERAPDF2.0Jets NNLO
 330 analysis as shown in Fig. 7 at the scale of $\mu_f = 10 \text{ GeV}^2$ and in Fig. 8 at the scale of $\mu_f = M_Z^2$.
 331 The reductions in the uncertainties for HERAPDF2.0Jets NNLO for $\alpha_s(M_Z^2) = 0.1155$ compared
 332 to $\alpha_s(M_Z^2) = 0.118$ are shown in Figs. 9 and 10. At high x and $\mu_f = M_Z^2$, the parameterisation
 333 uncertainties become important as can be seen by comparing Figs. 10 b) and 10 c).

334 The reduction in model and parameterisation uncertainty for $x < 10^{-3}$, compared to HERA-
335 PDF2.0 NNLO, is mostly due to the improved procedure to estimate this uncertainty. The ranges,
336 in which M_c and M_b were varied, were reduced but this had only little effect. The major effect
337 came from symmetrising the results of the variations of $\mu_{f_0}^2$ and M_c^2 as discussed in Section 3.3.
338 This removed a double counting of sources of uncertainty that had been present in the original
339 HERAPdf2.0 procedure. On the other hand, the reduction of experimental as well as model
340 and parameterisation uncertainties for $x > 10^{-3}$, is due to the influence of the jet data. This is
341 also demonstrated in Fig. 11, which shows ratios of the uncertainties with respect to the total
342 uncertainties of HERAPDF2.0 NNLO based on inclusive data only. Shown are the contributions
343 of the experimental, the experimental plus model, and the experimental plus parameterisation
344 uncertainties, with respect to the total uncertainties of HERAPDF2.0 NNLO, and the respective
345 reductions for HERAPDF2.0Jets NNLO. Selected other ratio plots are provided in Appendix B.

346 4.3 Comparisons of HERAPDF2.0Jets NNLO predictions to jet data

347 Comparisons of the predictions based on HERAPDF2.0Jets NNLO with fixed $\alpha_s(M_Z^2) = 0.1155$
348 to the data on jet production used as input to the fit are shown in Figs. 12 to 19. Each figure
349 presents in a) a direct comparison of the cross sections and in b) the respective ratios.

350 The uncertainties on the NNLO predictions as calculated by NNLOJET were taken into
351 account in all HERAPDF2.0Jets NNLO fits. The predictions based on the HERAPDF2.0Jets
352 NNLO PDFs were computed using the assumption of massless jets, i.e. the transverse energy,
353 E_T , and the transverse momentum of a jet, p_T , were assumed to be equivalent. For the inclusive
354 jet analyses, each jet p_T entered the cross section calculation separately. For dijet analyses, the
355 average of the transverse momenta, $\langle p_T \rangle$ was used. In these cases, $\langle p_T \rangle$ was also used to set the
356 factorisation and renormalisation scales to $\mu_f^2 = \mu_r^2 = Q^2 + \langle p_T \rangle^2$ for calculating predictions.
357 Scale uncertainties were not considered [16] for the comparisons to data. The predictions based
358 on the PDFs of HERAPDF2.0Jets NNLO clearly fit the data on jet production used as input very
359 well, showing that the inclusive data and jet production data both used as input to the NNLO
360 QCD fit are fully consistent.

361 5 Summary

362 The HERA DIS data set on inclusive ep scattering as published by the H1 and ZEUS col-
363 laborations [2], together with selected data on jet production, published separately by the two
364 collaborations, have been used as input to a pQCD analysis at NNLO.

365 An analysis was performed where $\alpha_s(M_Z^2)$ and the PDFs were fitted simultaneously. This
366 resulted in a value of $\alpha_s(M_Z^2) = 0.1156 \pm 0.0011$ (exp) $_{-0.0002}^{+0.0001}$ (model + parameterisation) \pm
367 0.0029 (scale). This result for $\alpha_s(M_Z^2)$ is compatible with the world average [24] and it is com-
368 petitive in comparison with other determinations at NNLO. The scale uncertainties were calcu-
369 lated under the assumption of fully correlated uncertainties between bins and data sets. They
370 would decrease to ± 0.0022 under the assumption of 50 % correlated and 50 % uncorrelated un-
371 certainties which is the value that can be directly compared to the previously published [2] scale
372 uncertainties of (+0.0037, -0.0030) observed in the HERAPDF2.0Jets NLO analysis.

373 Two sets of PDFs were determined for HERAPDF2.0Jets NNLO for fixed $\alpha_s(M_Z^2) = 0.1155$
374 and $\alpha_s(M_Z^2) = 0.118$. They are available to the community. Comparisons between the PDFs
375 of HERAPDF2.0Jets NNLO obtained for the two values of $\alpha_s(M_Z^2)$ were shown, as well as
376 comparisons to HERAPDF2.0 NNLO, for which jet data were not used as input to the fit. The
377 PDFs of HERAPDF2.0Jets NNLO and HERAPDF2.0 NNLO are consistent over the whole
378 kinematic range. This also demonstrates the consistency of the jet data and the inclusive data at
379 NNLO level. On balance, the inclusion of the jet data had two consequences: i) a lower value of
380 $\alpha_s(M_Z^2)$ is favoured; ii) the uncertainty on the gluon PDF was reduced. Predictions based on the
381 PDFs of HERAPDF2.0Jets NNLO were compared to the jet production data used as input. The
382 predictions describe the data very well.

383 The PDFs of HERAPDF2.0Jets NNLO complete the HERAPDF2.0 ensemble of parton dis-
384 tribution functions. This ensemble of PDFs, extracted from HERA data alone, presents a con-
385 sistent picture in the framework of pQCD. It is one of the legacies of HERA.

386 **6 Acknowledgements**

387 We are grateful to the HERA machine group whose outstanding efforts have made the H1 and
388 ZEUS experiments possible. We appreciate the contributions to the construction, maintenance
389 and operation of the H1 and ZEUS detectors of many people who are not listed as authors.
390 We thank our funding agencies for financial support, the DESY technical staff for continuous
391 assistance and the DESY directorate for their support and for the hospitality they extended to
392 the non-DESY members of the collaborations. We would like to give credit to all partners
393 contributing to the EGI computing infrastructure for their support. We acknowledge the support
394 of the IPPP Associateship program for this project. One of the authors, A. Cooper-Sarkar, would
395 like to thank the Leverhulme Foundation for their support.

References

- 396
- 397 [1] A. Cooper-Sarkar and R. Devenish, *Deep inelastic Scattering*, Oxford Univ. Press (2011),
398 ISBN 978-0-19-960225-4.
- 399 [2] H. Abramowicz *et al.*, [H1 and ZEUS Collaborations], *Eur. Phys. J. C* **75**, 580 (2015),
400 [arXiv:1506.06042].
- 401 [3] V. N. Gribov and L. N. Lipatov, *Sov. J. Nucl. Phys.* **15**, 438 (1972).
- 402 [4] V. N. Gribov and L. N. Lipatov, *Sov. J. Nucl. Phys.* **15**, 675 (1972).
- 403 [5] L. N. Lipatov, *Sov. J. Nucl. Phys.* **20**, 94 (1975).
- 404 [6] Y. L. Dokshitzer, *Sov. Phys. JETP* **46**, 641 (1977).
- 405 [7] G. Altarelli and G. Parisi, *Nucl. Phys. B* **126**, 298 (1977).
- 406 [8] B. Fanchiotti, S. Kniehl and A. Sirlin, *Phys. Rev. D* **48**, 307 (1993), [hep-ph/9803393].
- 407 [9] A. Aktas *et al.* [H1 Collaboration], *Phys. Lett. B* **653**, 134 (2007), [arXiv:0706.3722].
- 408 [10] F. Aaron *et al.* [H1 Collaboration], *Eur. Phys. J. C* **67**, 1 (2010), [arXiv:0911.5678].
- 409 [11] S. Chekanov *et al.* [ZEUS Collaboration], *Phys. Lett. B* **547**, 164 (2002), [hep-
410 ex/0208037].
- 411 [12] H. Abramowicz *et al.* [ZEUS Collaboration], *Eur. Phys. J. C* **70**, 965 (2010),
412 [arXiv:1010.6167].
- 413 [13] V. Andreev *et al.* [H1 Collaboration], *Eur. Phys. J. C* **77**, 215 (2017), [Erratum: *Eur. Phys.*
414 *J. C* **81**, 739 (2021)], [1611.03421].
- 415 [14] V. Andreev *et al.* [H1 Collaboration], *Eur. Phys. J. C* **65**, 2 (2015), [arXiv:1406.4709].
- 416 [15] J. Currie, T. Gehrmann, and J. Niehues, *Phys. Rev. Lett.* **117**, 042001 (2016),
417 [arXiv:1606.03991].
- 418 [16] J. Currie, T. Gehrmann, A. Huss, and J. Niehues, *JHEP* **07**, 018 (2017), [Erratum: *JHEP*
419 **12**, 042 (2020)], [1703.05977].
- 420 [17] T. Gehrmann *et al.*, in *The Proceedings of the 13th International Symposium on Radiative*
421 *Corrections (RADCOR2017), St. Gilgen, Austria* (2017), vol. 1707, [arXiv:1801.06415].
- 422 [18] T. Kluge, K. Rabbertz, and M. Wobisch (2006), [hep-ph/0609285].
- 423 [19] Britzger.D *et al.*, in *20th International Workshop on Deep-Inelastic Scattering and Related*
424 *Subjects (DIS 2012): Bonn, Germany* (2012), p. 217, [arXiv:1208.3641].
- 425 [20] D. Britzger *et al.*, at *DIS 2014* (2014), URL [http://indico.cern.ch/event/258017/
426 session/1/contribution/202](http://indico.cern.ch/event/258017/session/1/contribution/202).
- 427 [21] T. Carli, G. Salam, and F. Siegert (2005), [arXiv:0510324].

- 428 [22] T. Carli *et al.*, Eur. Phys. J. C **66**, 503 (2010), [arXiv:0911.2985].
- 429 [23] V. Andreev *et al.* [H1 Collaboration], Eur. Phys. J. C **77**, 791 (2017).
- 430 [24] M. Tanabashi *et al.* (Particle Data Group), Phys. Rev. D **98**, 030001 (2018).
- 431 [25] R. S. Thorne and R. G. Roberts, Phys. Rev. D **57**, 6871 (1998), [hep-ph/9709442].
- 432 [26] R. S. Thorne, Phys. Rev. D **73**, 054019 (2006), [hep-ph/0601245].
- 433 [27] R. S. Thorne, Phys. Rev. D **86**, 074017 (2012), [arXiv:1201.6180].
- 434 [28] H. Abramowicz *et al.*, [H1 and ZEUS Collaborations], Eur. Phys. J. C **78**, 473 (2018),
435 [arXiv:1804.01019].
- 436 [29] F. D. Aaron *et al.*, [H1 and ZEUS Collaborations], Eur. Phys. J. C **73**, 2311 (2013),
437 [arXiv:1211.1182].
- 438 [30] M. Botje, Comp. Phys. Comm. **182**, 490 (2011), [arXiv:1005.1481].
- 439 [31] S. Alekhin *et al.* (2014), [arXiv:1410.4412].
- 440 [32] H. Spiesberger, in *Proc. of Future Physics at HERA*, edited by G. Ingelman, A. De Roeck
441 and R. Klanner (1995), p. 227.
- 442 [33] F. Aaron *et al.*, [H1 and ZEUS Collaborations], JHEP **1001**, 109 (2010),
443 [arXiv:0911.0884].
- 444 [34] A. D. Martin, W. J. Stirling, R. S. Thorne, and G. Watt, Eur. Phys. J. C **63**, 189 (2009),
445 [arXiv:0901.0002].
- 446 [35] P. M. Nadolsky *et al.*, Phys. Rev. D **78**, 013004 (2008), [arXiv:0802.0007].
- 447 [36] M. Aaboud *et al.*, Eur. Phys. J. C **77**, 367 (2017), [arXiv:1612.03016].
- 448 [37] V. Andreev *et al.* [H1 Collaboration], Eur. Phys. J. C **77**, 791 (2017), [Erratum: Eur. Phys.
449 J. C **81**, 738 (2021)], [1709.07251].
- 450 [38] D. Britzger *et al.* [NNLOJet and Applfast Collaboration], Eur. Phys. J. C **79**, 845 (2019),
451 [arXiv:1906.05303].
- 452 [39] S. Forte and Z. Kassabov, Eur. Phys. J. C **80**, 182 (2020), [arXiv:2001.04986].
- 453 [40] J. Beringer *et al.* (Particle Data Group), Phys. Rev. D **86**, 010001 (2012).
- 454 [41] The combined data together with the full correlation information and the grids for HERA-
455 PDF2.0 are provided at URL <http://www.desy.de/h1zeus/herapdf20/>.

Data set	taken		Q^2 [GeV ²] range		\mathcal{L} pb ⁻¹	e^+/e^-	\sqrt{s} GeV	norma- lised	all points	used points	Ref.
	from	to	from	to							
H1 HERA I normalised jets	1999	2000	150	15000	65.4	e^+p	319	yes	24	24	[9]
H1 HERA I jets at low Q^2	1999	2000	5	100	43.5	e^+p	319	no	28	20	[10]
H1 normalised inclusive jets at high Q^2	2003	2007	150	15000	351	e^+p/e^-p	319	yes	30	30	[13,14]
H1 normalised dijets at high Q^2	2003	2007	150	15000	351	e^+p/e^-p	319	yes	24	24	[14]
H1 normalised inclusive jets at low Q^2	2005	2007	5.5	80	290	e^+p/e^-p	319	yes	48	37	[13]
H1 normalised dijets at low Q^2	2005	2007	5.5	80	290	e^+p/e^-p	319	yes	48	37	[13]
ZEUS inclusive jets	1996	1997	125	10000	38.6	e^+p	301	no	30	30	[11]
ZEUS dijets	1998–2000 &	2004–2007	125	20000	374	e^+p/e^-p	318	no	22	16	[12]

Table 1: The data sets on jet production from H1 and ZEUS used for the HERAPDF2.0Jets NNLO fits. The term normalised indicates that all cross sections are normalised to the respective NC inclusive cross sections.

Parameter	Central value	Downwards variation	Upwards variation
Q_{\min}^2 [GeV ²]	3.5	2.5	5.0
f_s	0.4	0.3	0.5
M_c [GeV]	1.41	1.37*	1.45
M_b [GeV]	4.20	4.10	4.30
μ_{f0}^2 [GeV ²]	1.9	1.6	2.2*

Table 2: Central values of model input parameters and their one-sigma variations. It was not possible to implement the variations marked * because $\mu_{f0} < M_c$ is required, see Section 3.3. In these cases, the uncertainty on the PDF obtained from the other variation was symmetrised.

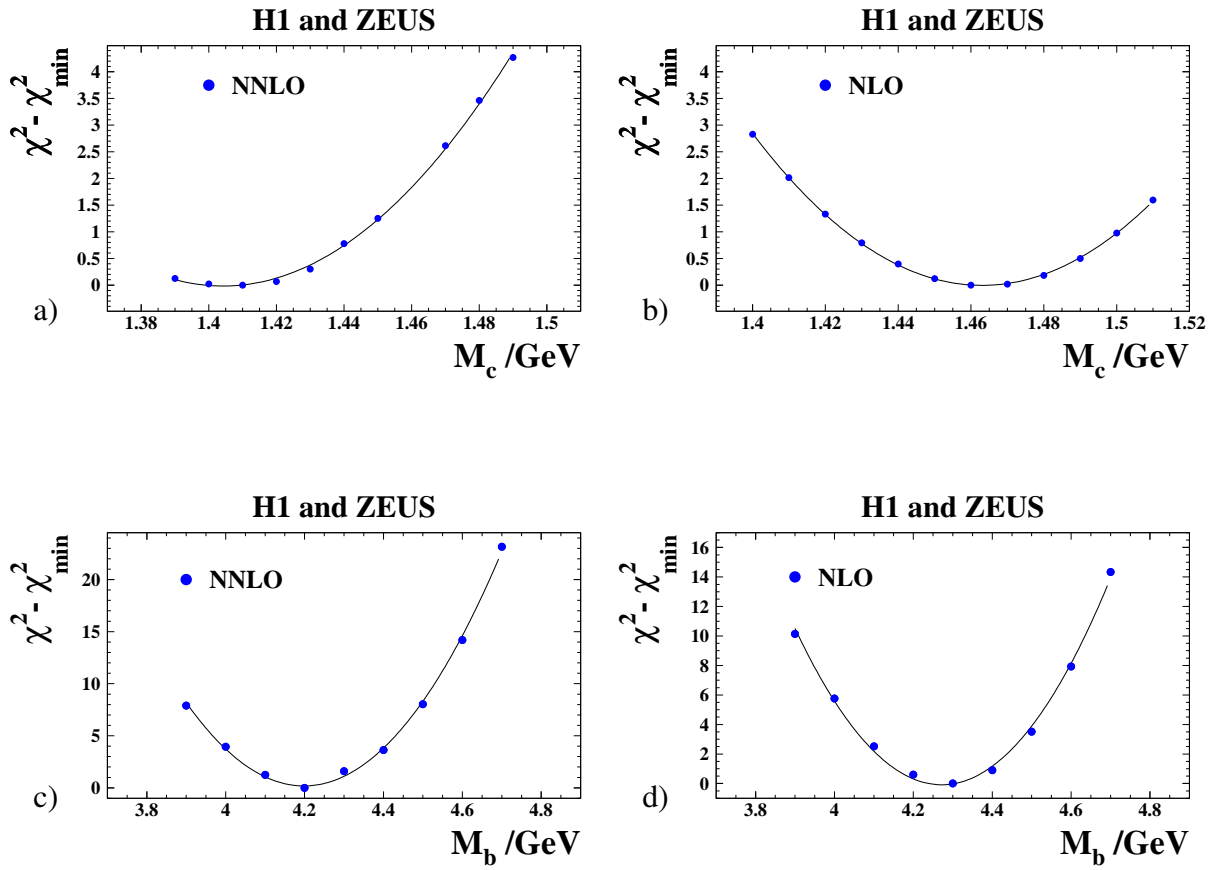


Figure 1: $\Delta\chi^2 = \chi^2 - \chi_{\min}^2$ vs. a) and b) M_c with $M_b = 4.2$ GeV, and c) and d) M_b with $M_c = 1.41$ GeV for a) and c) HERAPDF2.0Jets NNLO fits with fixed $\alpha_s(M_Z^2) = 0.1155$ and b) and d) the corresponding NLO fits for $M_c = 1.46$ GeV, $M_b = 4.3$ GeV and $\alpha_s(M_Z^2) = 0.118$.

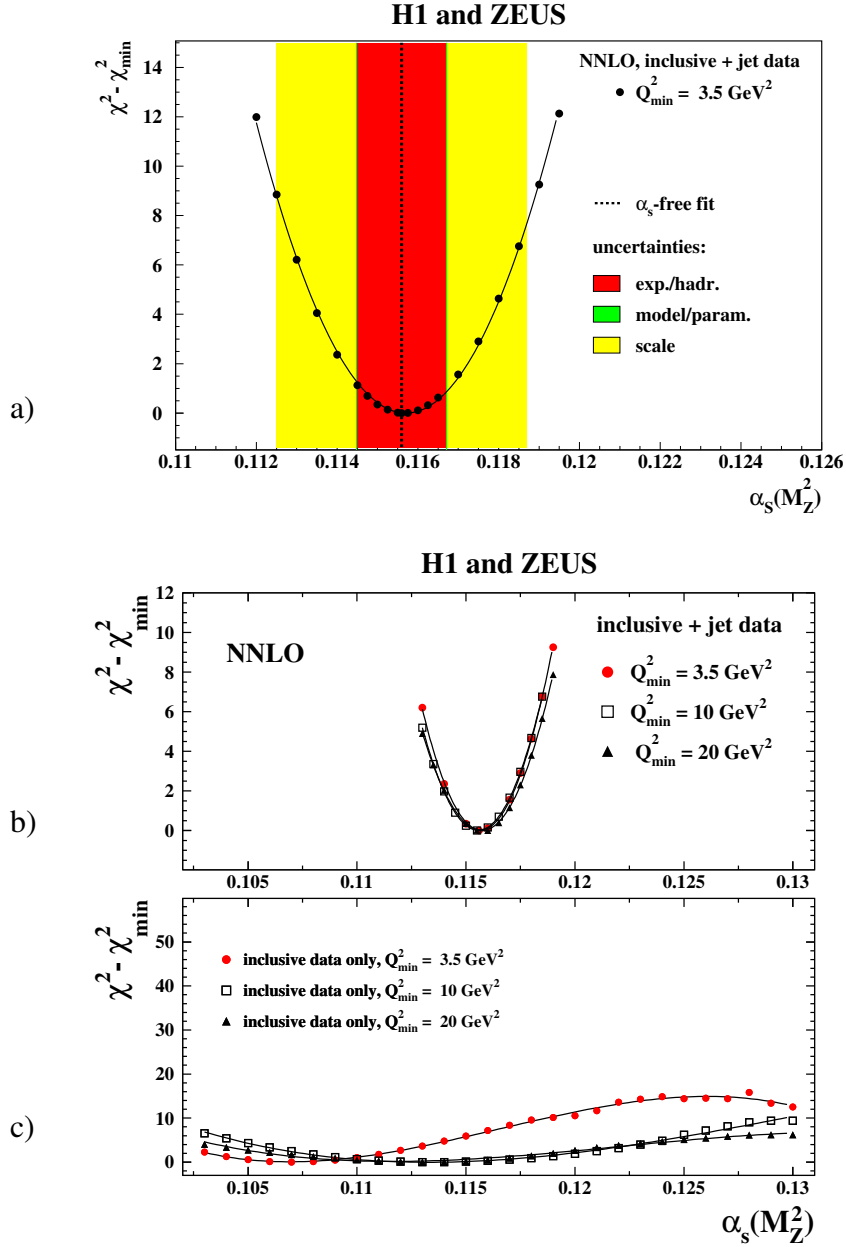


Figure 2: $\Delta\chi^2 = \chi^2 - \chi_{\min}^2$ vs. $\alpha_s(M_Z^2)$ for HERAPDF2.0Jets NNLO fits with fixed $\alpha_s(M_Z^2)$ with a) the standard Q_{\min}^2 of 3.5 GeV^2 b) with Q_{\min}^2 set to 3.5 GeV^2 , 10 GeV^2 and 20 GeV^2 for the inclusive data. In a), the result and all uncertainties determined for the HERAPDF2.0Jets NNLO fit with free $\alpha_s(M_Z^2)$ are also shown, added in quadrature. In b), not all scan points for Q_{\min}^2 of 3.5 GeV^2 are plotted for better visibility. c) For comparison, the situation for fits to only inclusive data is shown, taken from [2].

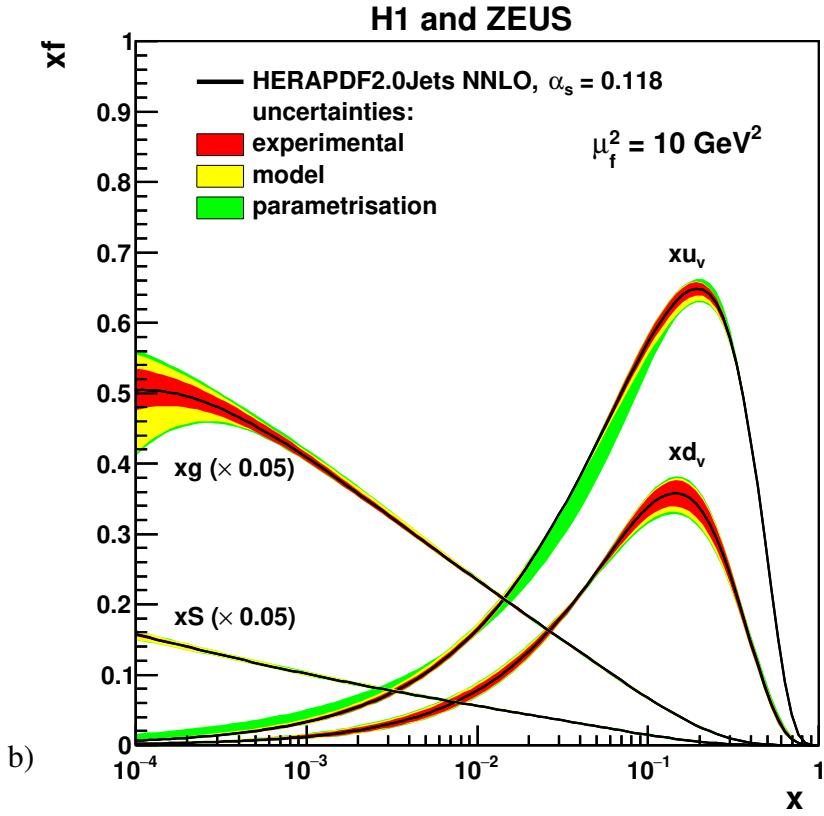
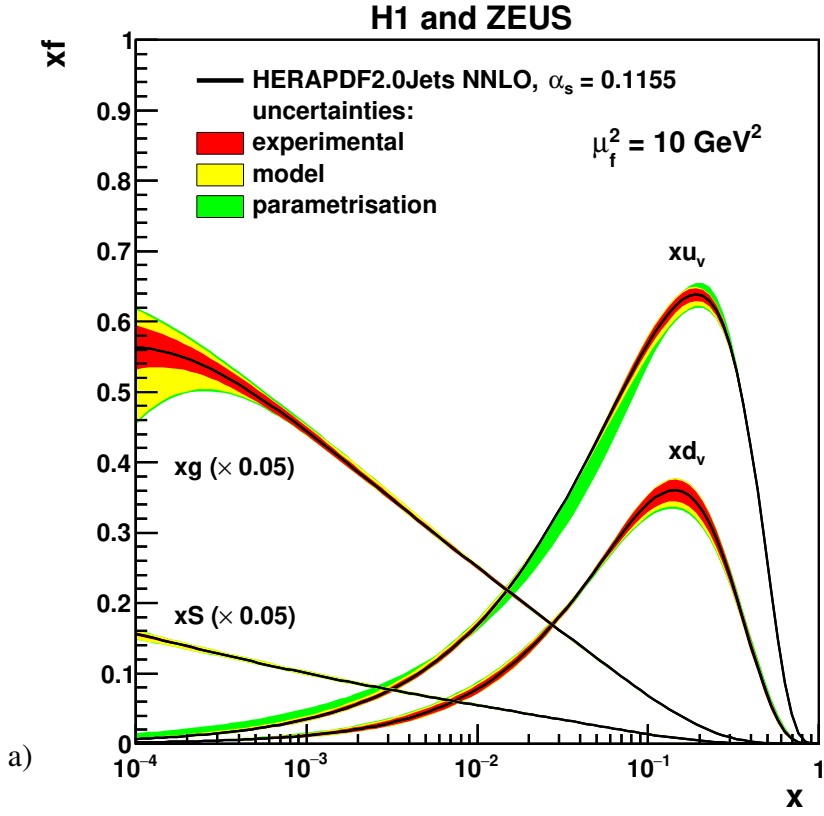


Figure 3: The parton distribution functions xu_v , xd_v , xg and $xS = x(\bar{U} + \bar{D})$ of HERAPDF2.0Jets NNLO, with a) $\alpha_s(M_Z^2)$ fixed to 0.1155 and b) $\alpha_s(M_Z^2)$ fixed to 0.118 at the scale $\mu_f^2 = 10 \text{ GeV}^2$. The uncertainties are shown as differently shaded bands.

H1 and ZEUS

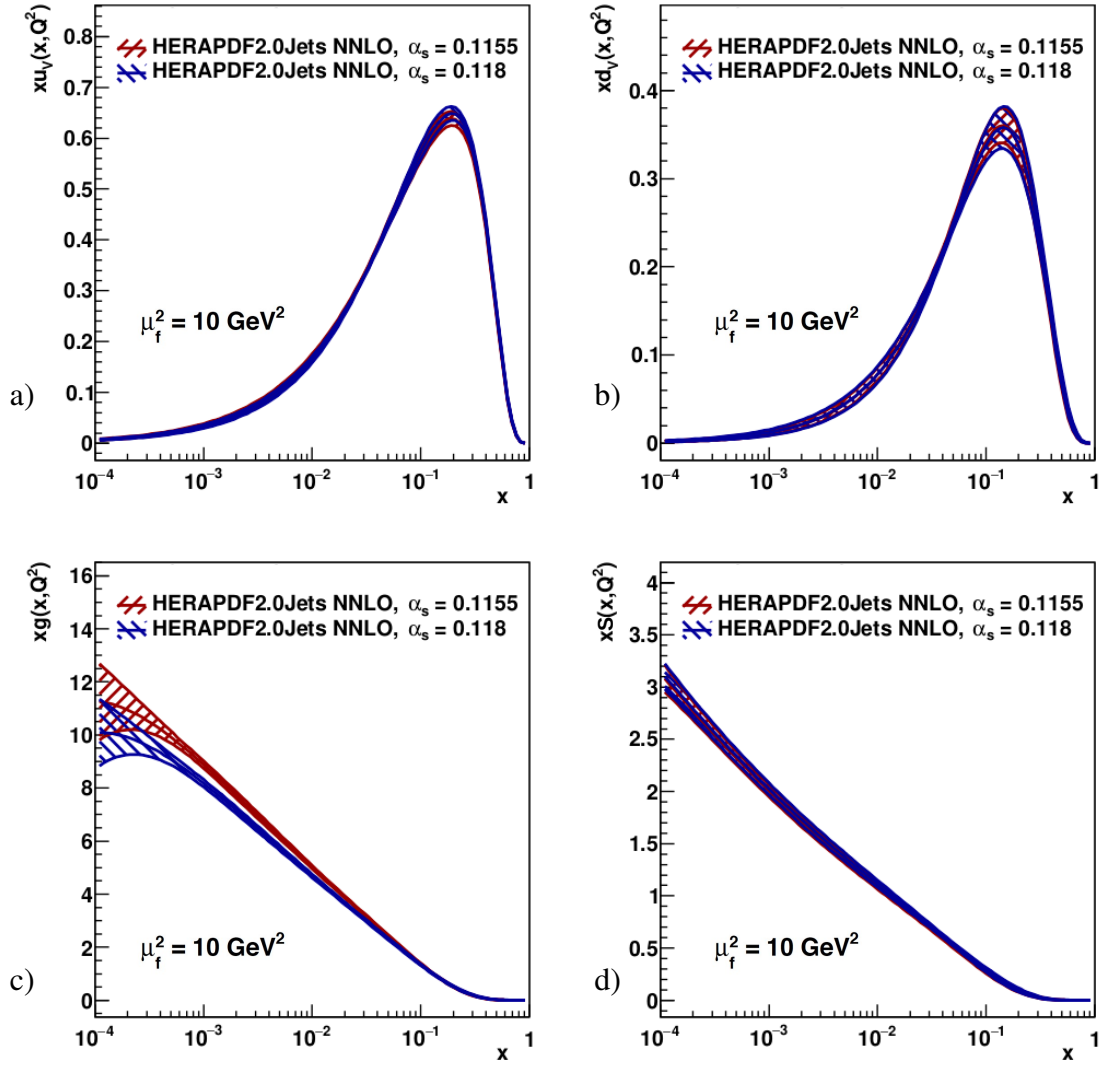


Figure 4: Comparison of the parton distribution functions a) xu_v , b) xd_v , c) xg and d) $xS = x(\bar{U} + \bar{D})$ of HERAPDF2.0Jets NNLO with fixed $\alpha_s(M_Z^2) = 0.1155$ and $\alpha_s(M_Z^2) = 0.118$ at the scale $\mu_f^2 = 10 \text{ GeV}^2$. The total uncertainties are shown as differently hatched bands.

H1 and ZEUS

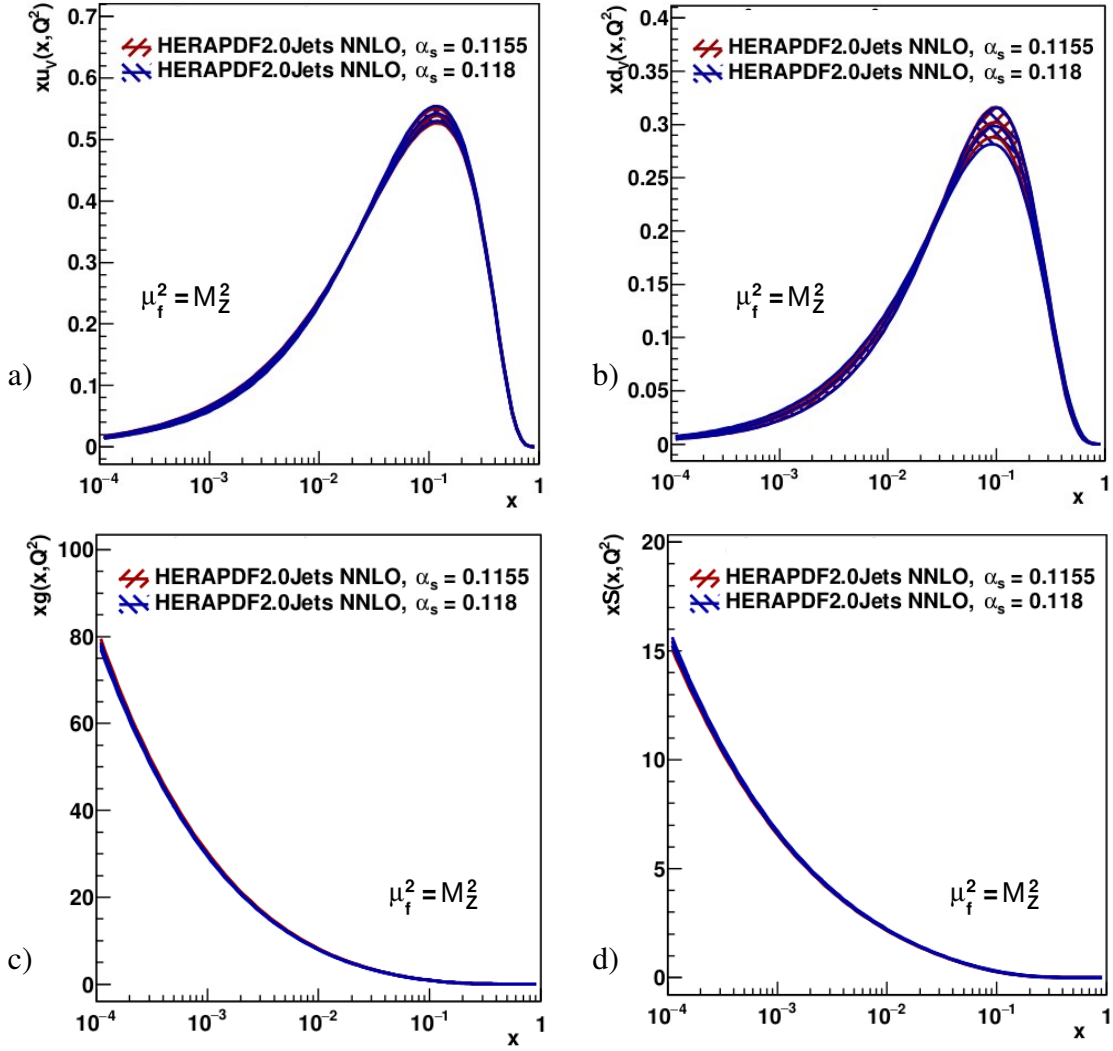


Figure 5: Comparison of the parton distribution functions a) xu_v , b) xd_v , c) xg and d) $xS = x(\bar{U} + \bar{D})$ of HERAPDF2.0Jets NNLO with fixed $\alpha_s(M_Z^2) = 0.1155$ and $\alpha_s(M_Z^2) = 0.118$ at the scale $\mu_f^2 = M_Z^2$ with $M_Z = 91.19$ GeV [24]. The total uncertainties are shown as differently hatched bands.

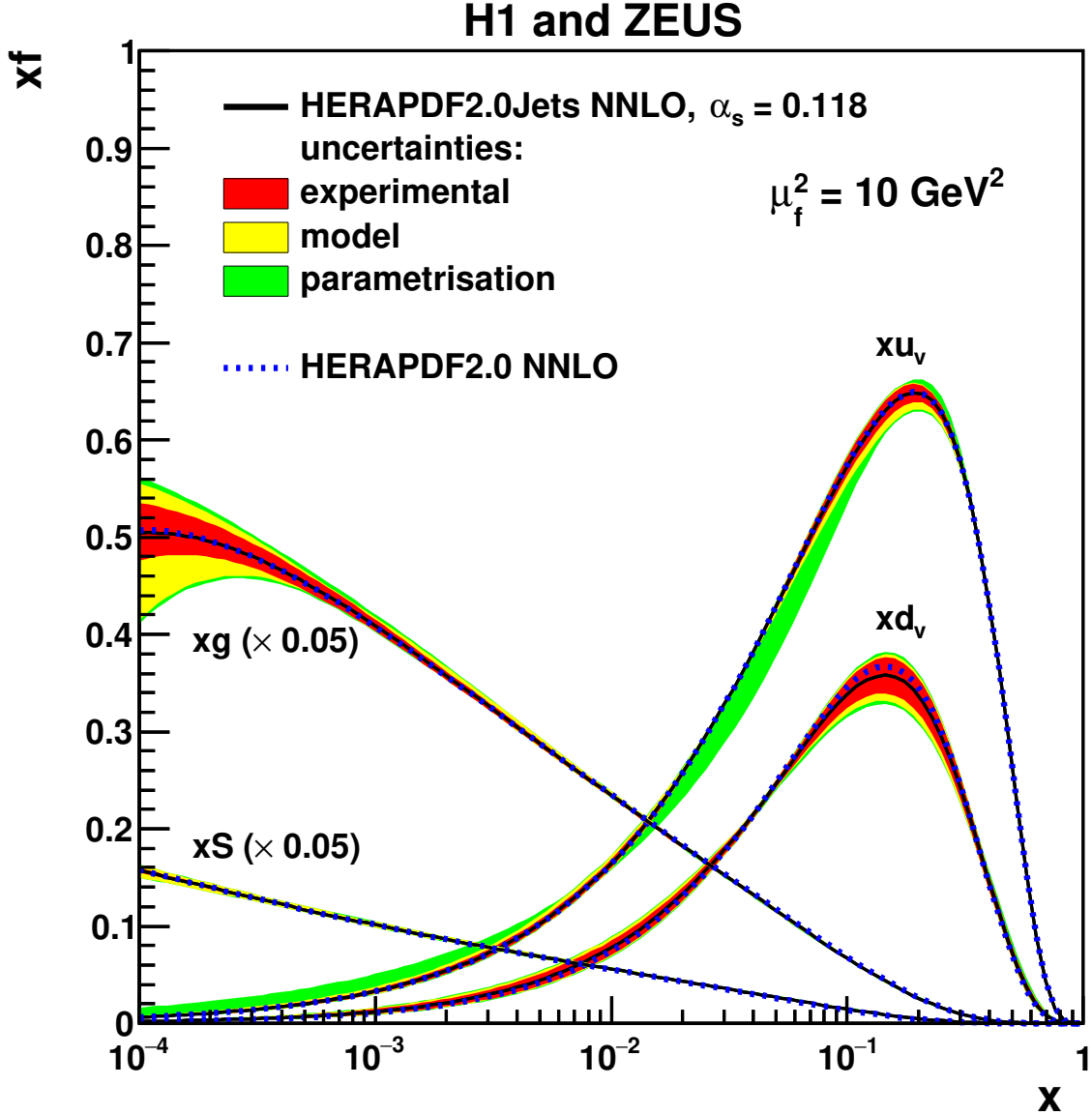


Figure 6: Comparison of the parton distribution functions xu_v , xd_v , xg and $xS = x(\bar{U} + \bar{D})$ of HERAPDF2.0Jets NNLO and HERAPDF2.0 NNLO, which was based on inclusive data only, both with fixed $\alpha_s(M_Z^2) = 0.118$, at the scale $\mu_f^2 = 10 \text{ GeV}^2$. The full uncertainties of HERAPDF2.0Jets NNLO are shown as differently shaded bands and the central value of HERAPDF2.0 NNLO is shown as a dotted line.

H1 and ZEUS

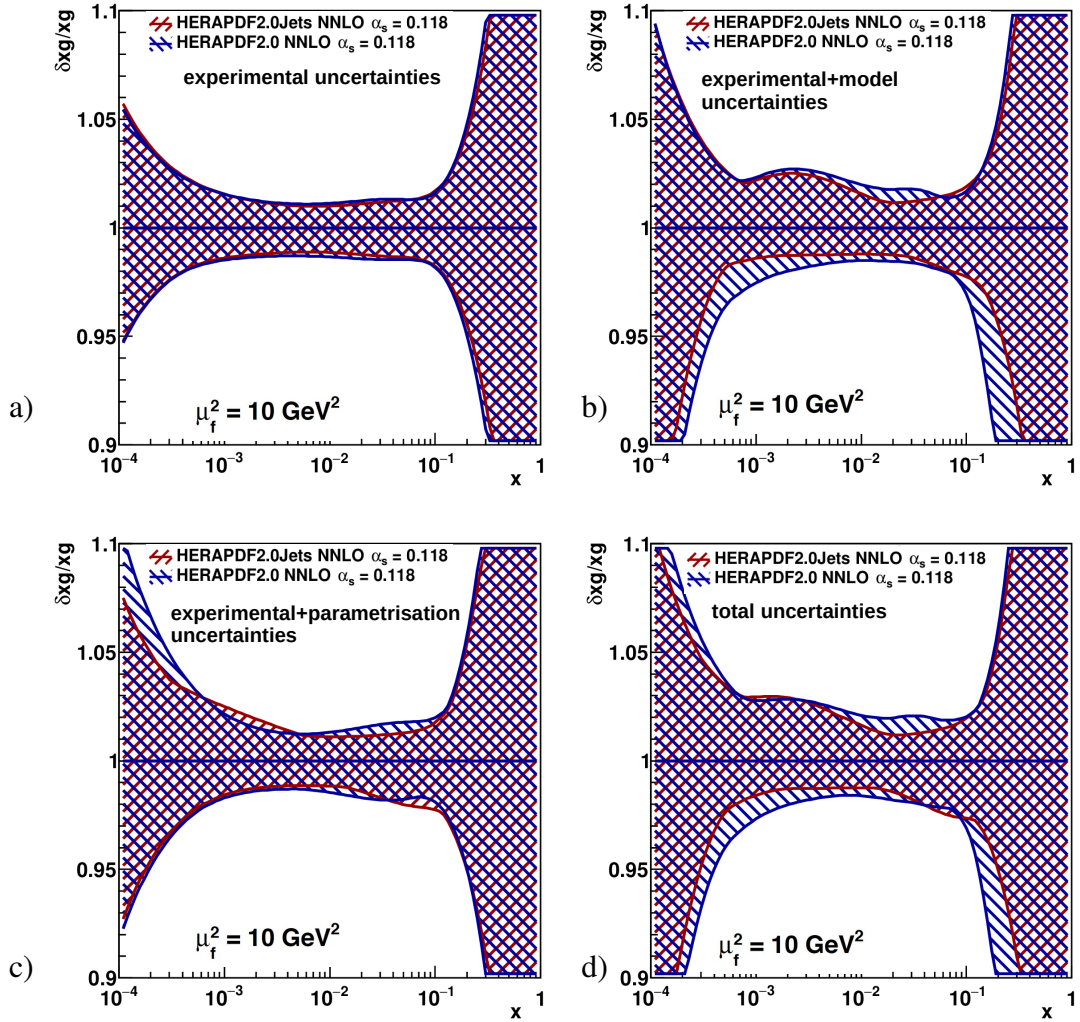


Figure 7: Comparison of the normalised uncertainties on the gluon PDFs of HERAPDF2.0Jets NNLO and HERAPDF2.0 NNLO for a) experimental, i.e. fit, b) experimental plus model, c) experimental plus parameterisation, d) total uncertainties at the scale $\mu_f^2 = 10 \text{ GeV}^2$. The uncertainties on both gluon PDFs are shown as differently hatched bands.

H1 and ZEUS

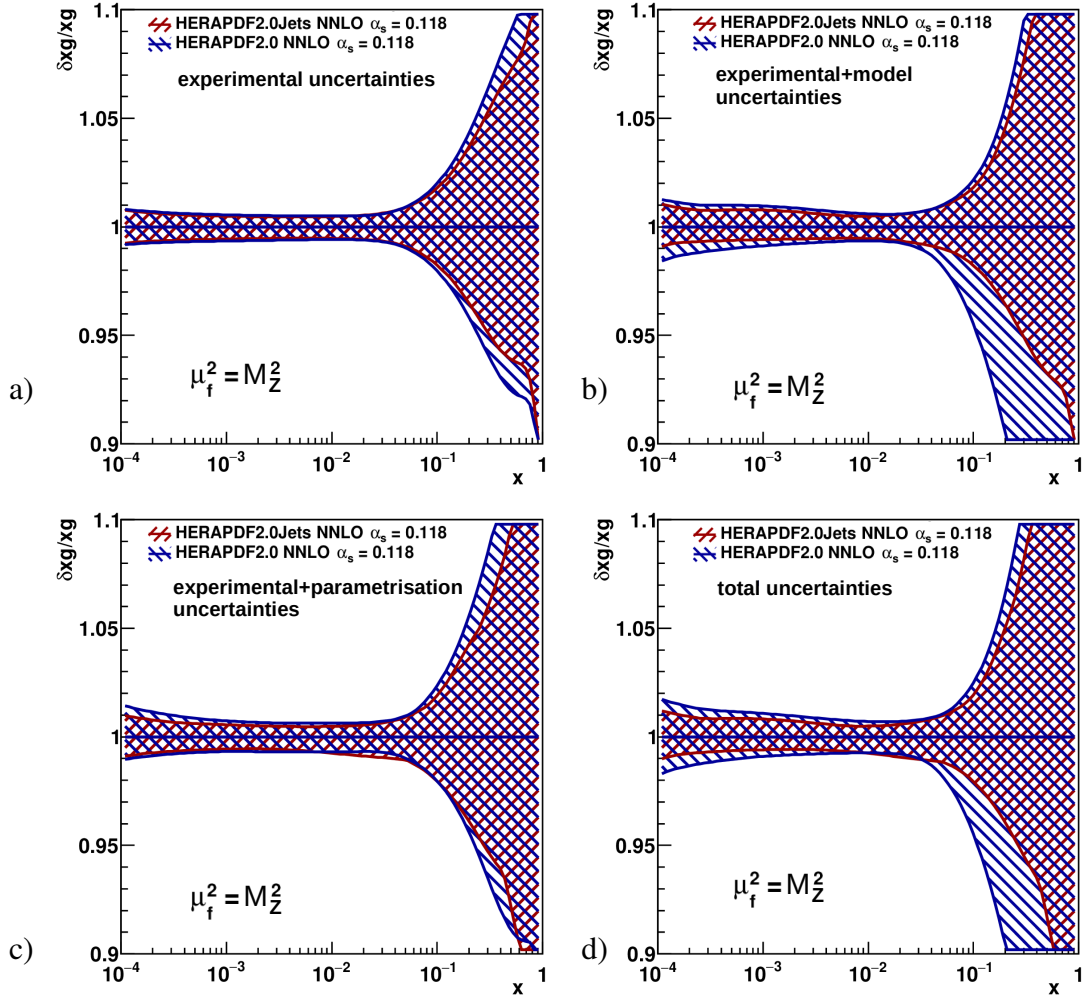


Figure 8: Comparison of the normalised uncertainties on the gluon PDFs of HERAPDF2.0Jets NNLO and HERAPDF2.0 NNLO for a) experimental, i.e. fit, b) experimental plus model, c) experimental plus parameterisation, d) total uncertainties at the scale $\mu_f^2 = M_Z^2$. The uncertainties on both gluon PDFs are shown as differently hatched bands.

H1 and ZEUS

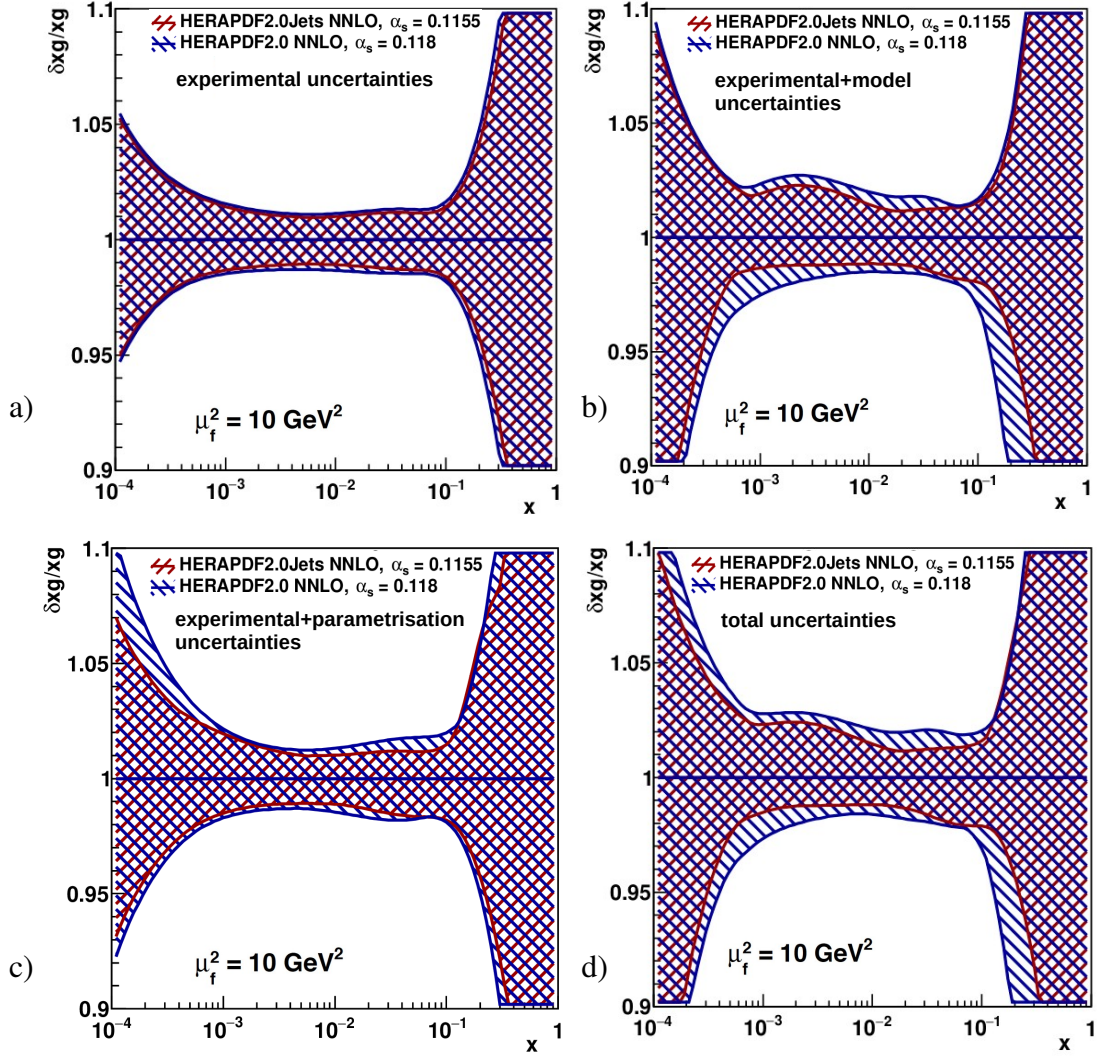


Figure 9: Comparison of the normalised uncertainties on the gluon PDFs of HERAPDF2.0Jets NNLO and HERAPDF2.0 NNLO for a) experimental, i.e. fit, b) experimental plus model, c) experimental plus parameterisation, d) total uncertainties at the scale $\mu_f^2 = 10 \text{ GeV}^2$. The uncertainties on both gluon PDFs are shown as differently hatched bands.

H1 and ZEUS

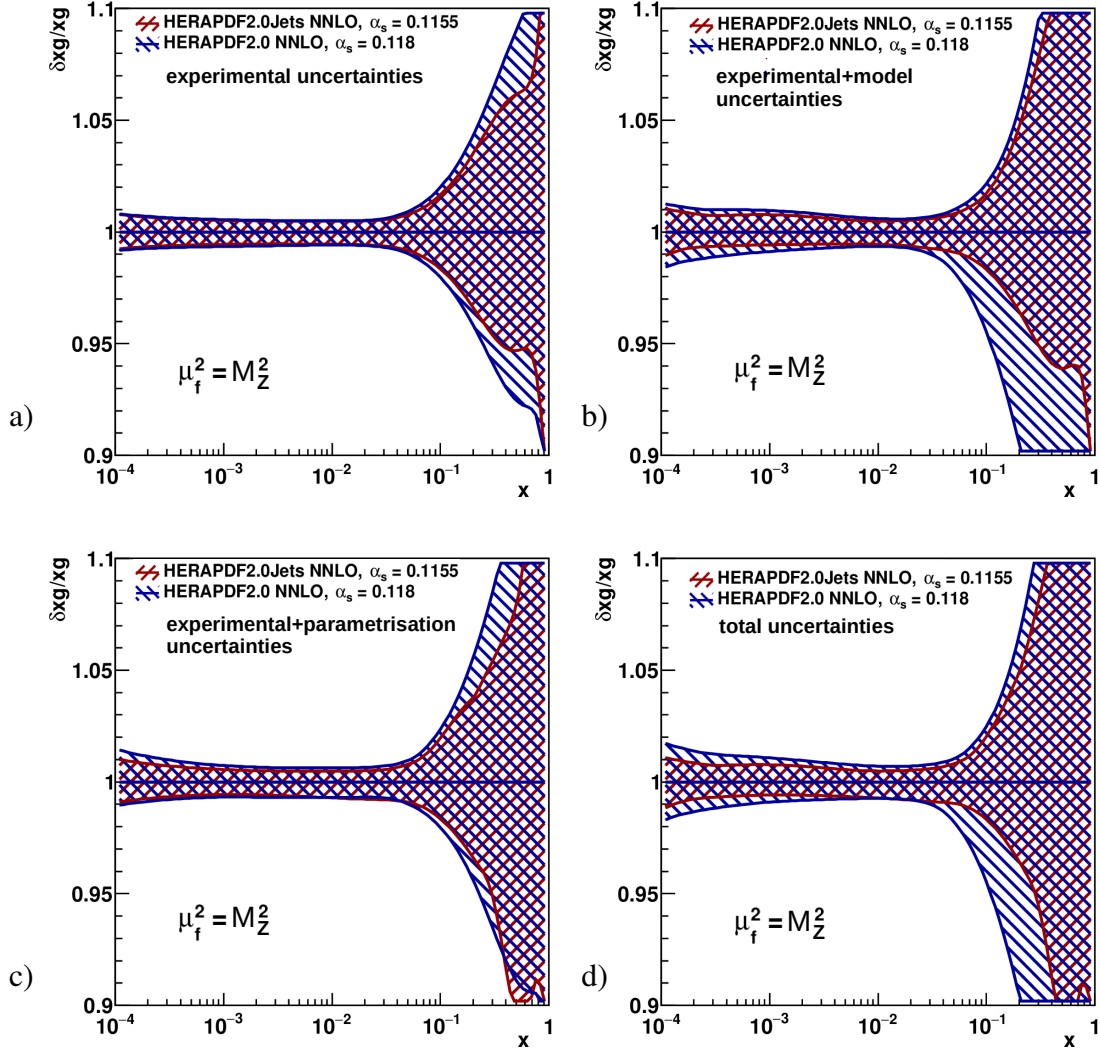


Figure 10: Comparison of the normalised uncertainties on the gluon PDFs of HERAPDF2.0Jets NNLO and HERAPDF2.0 NNLO for a) experimental, i.e. fit, b) experimental plus model, c) experimental plus parameterisation, a) total uncertainties at the scale $\mu_f^2 = M_Z^2$. The uncertainties on both gluon PDFs are shown as differently hatched bands.

H1 and ZEUS

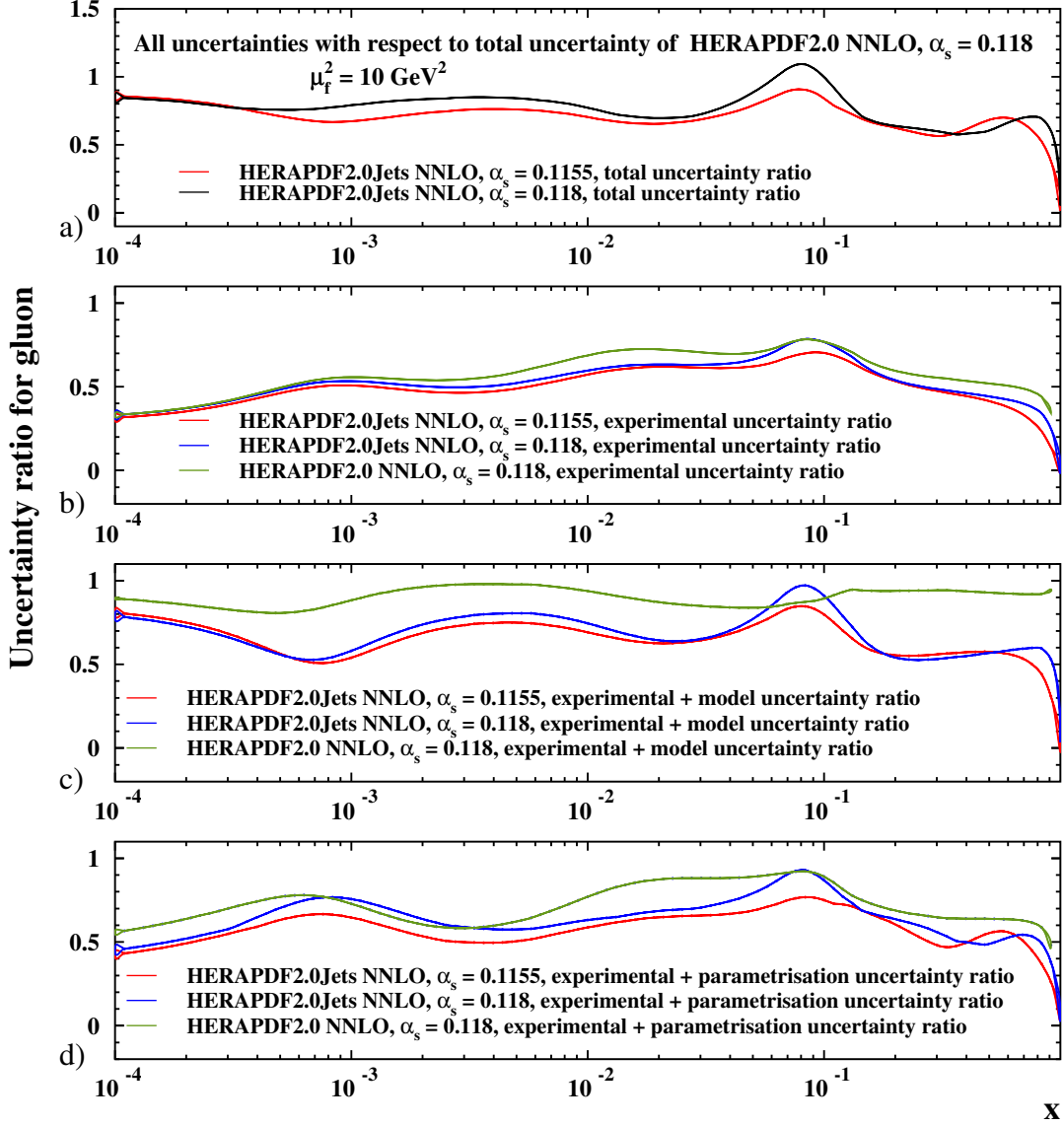


Figure 11: Ratios of uncertainties relative to the total uncertainties of HERAPDF2.0 NNLO $\alpha_s(M_Z^2) = 0.118$ a) total, b) experimental, c) experimental plus model, d) experimental plus parametrisation uncertainties for HERAPDF2.0Jets NNLO $\alpha_s(M_Z^2) = 0.118$ and $\alpha_s(M_Z^2) = 0.1155$ at the scale $\mu_f^2 = 10 \text{ GeV}^2$.

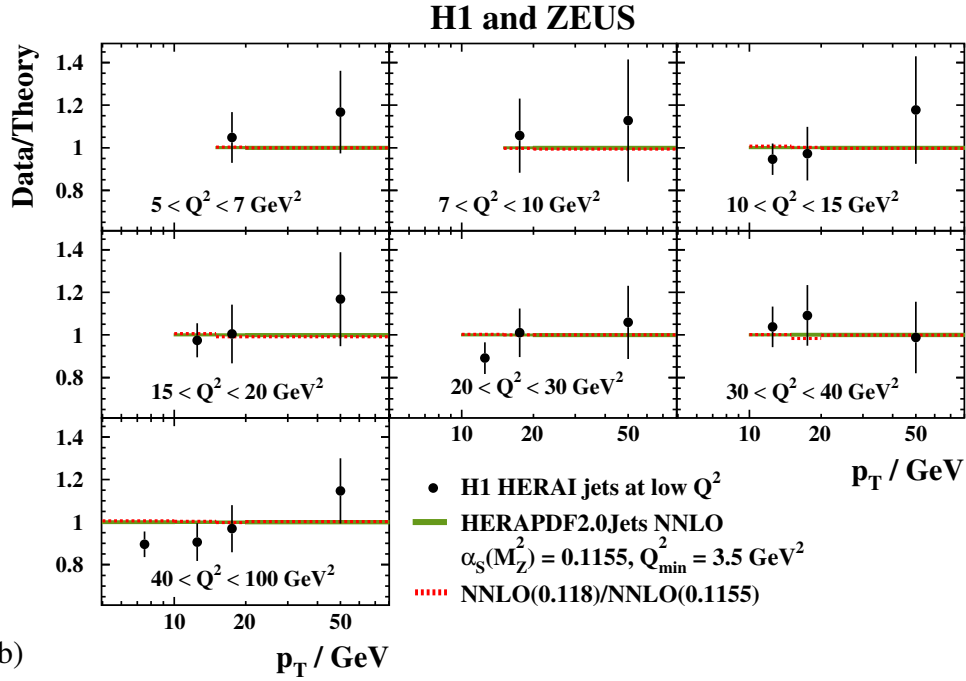
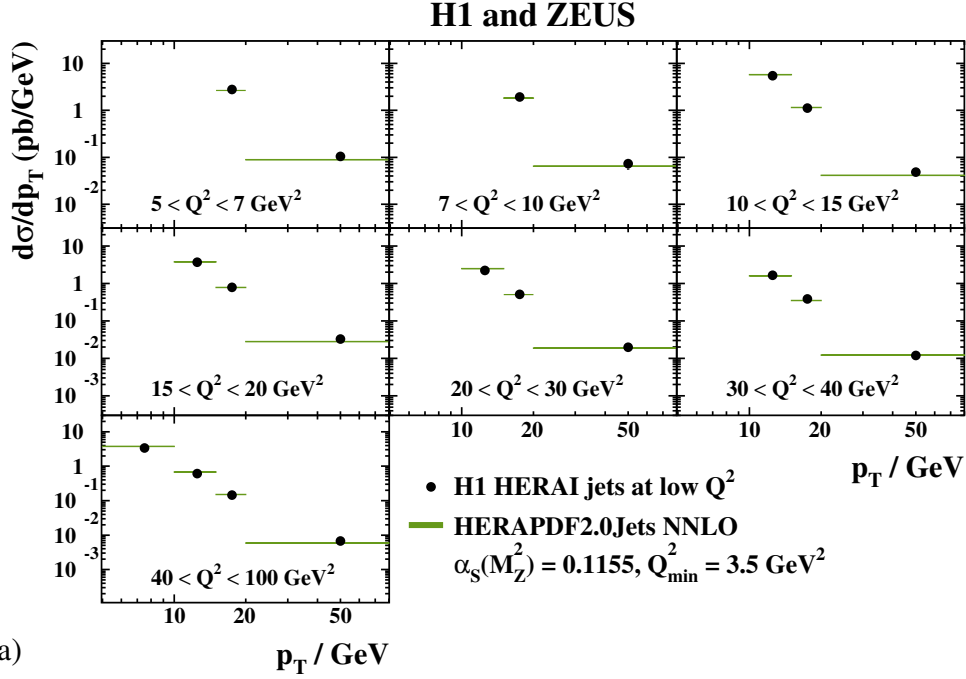


Figure 12: a) Differential jet cross sections, $d\sigma/dp_T$, in bins of Q^2 between 5 and 100 GeV^2 as measured by H1. Also shown are predictions based on HERAPDF2.0Jets NNLO. The bands represent the total uncertainties on the predictions excluding scale uncertainties, the bands are mostly invisible. Only data used in the fit are shown. b) Measured cross sections divided by predictions based on HERAPDF2.0Jets NNLO.

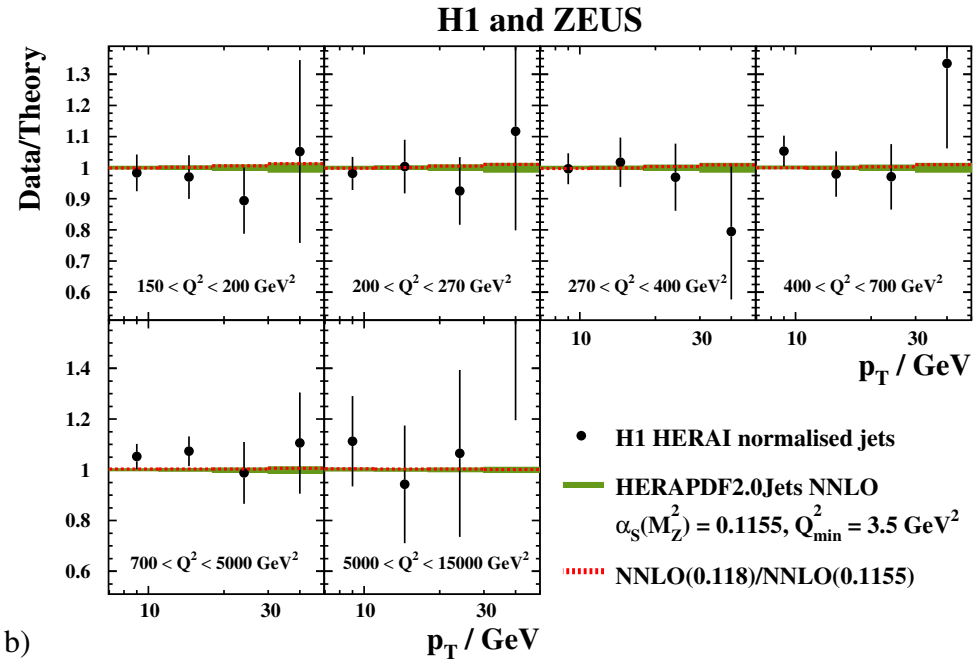
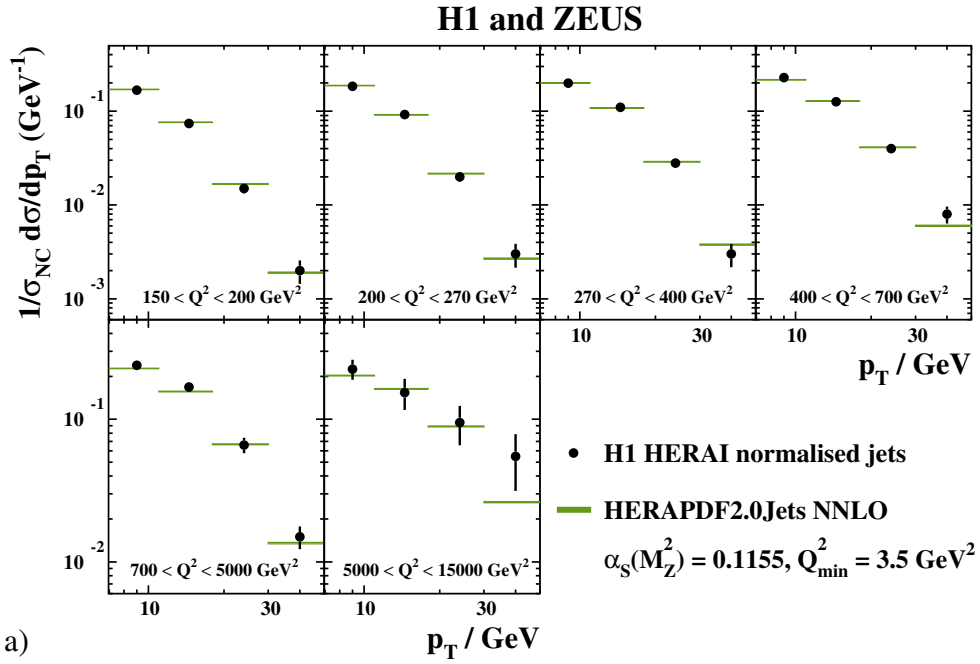


Figure 13: a) Differential jet cross sections, $d\sigma/dp_T$, normalised to NC inclusive cross sections, in bins of Q^2 between 150 and 15000 GeV^2 as measured by H1. Also shown are predictions based on HERAPDF2.0Jets NNLO. The bands represent the total uncertainties on the predictions excluding scale uncertainties; the bands are mostly invisible. Only data used in the fit are shown. b) Measured cross sections divided by predictions based on HERAPDF2.0Jets NNLO.

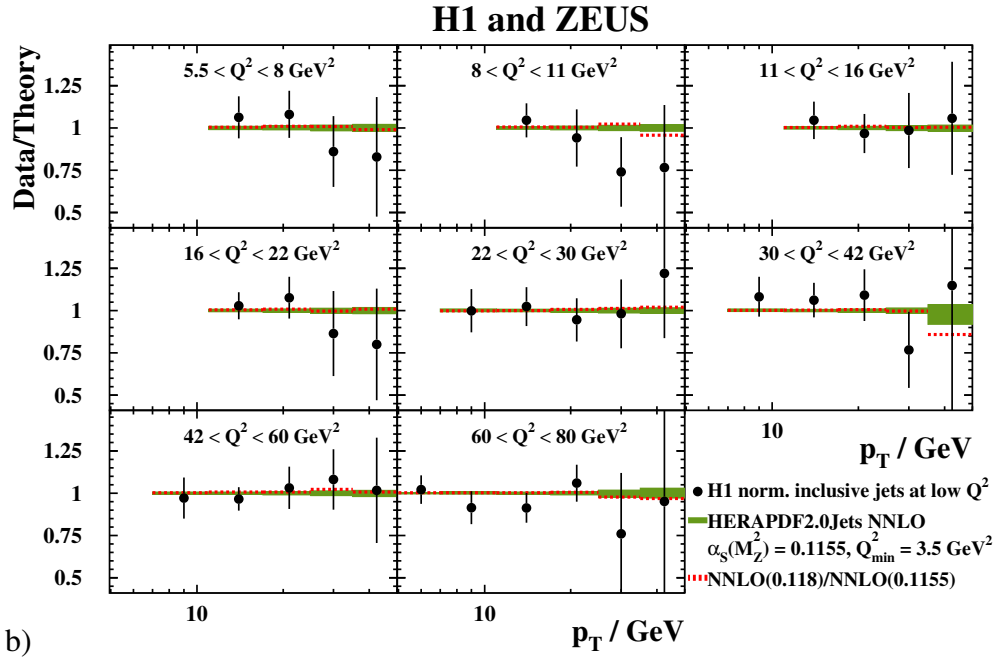
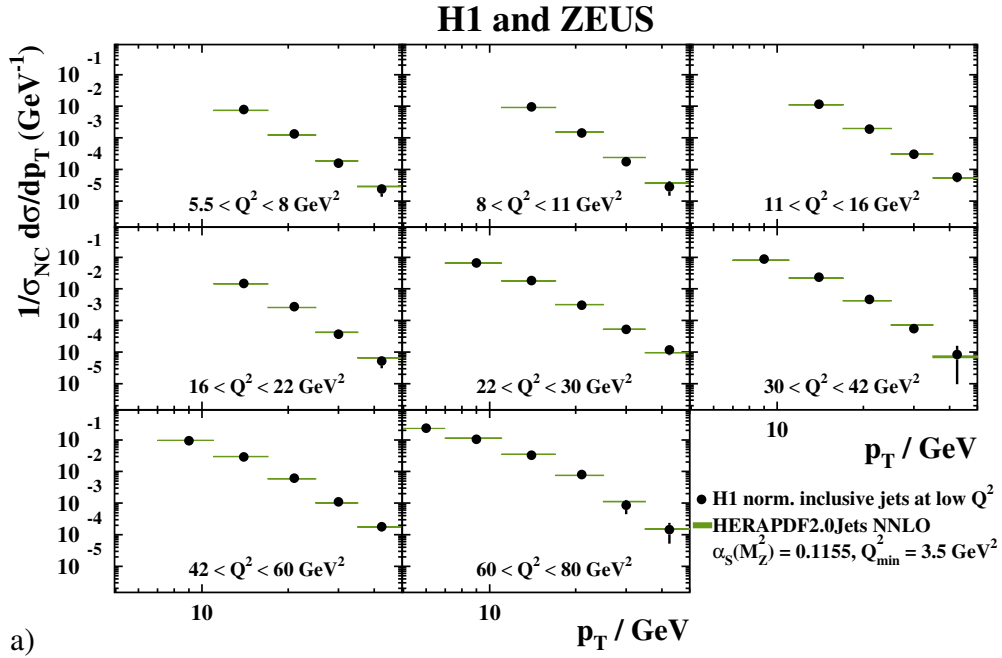


Figure 14: a) Differential jet cross sections, $d\sigma/dp_T$, normalised to NC inclusive cross sections, in bins of Q^2 between 5 and 80 GeV^2 as measured by H1. Also shown are predictions based on HERAPDF2.0Jets NNLO. The bands represent the total uncertainties on the predictions excluding scale uncertainties; the bands are mostly invisible. Only data used in the fit are shown. b) Measured cross sections divided by predictions based on HERAPDF2.0Jets NNLO.

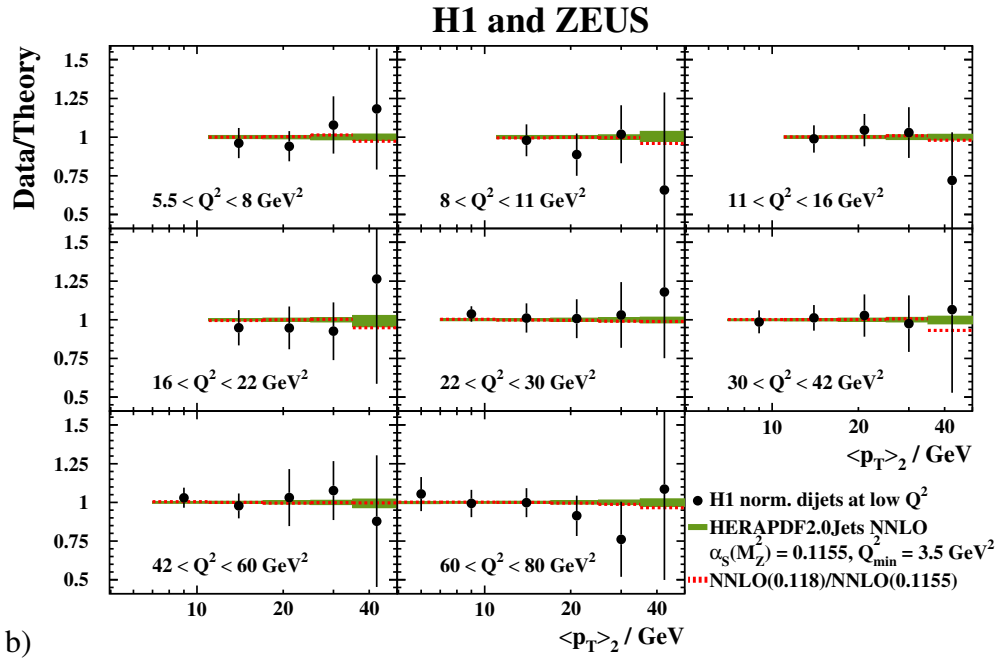
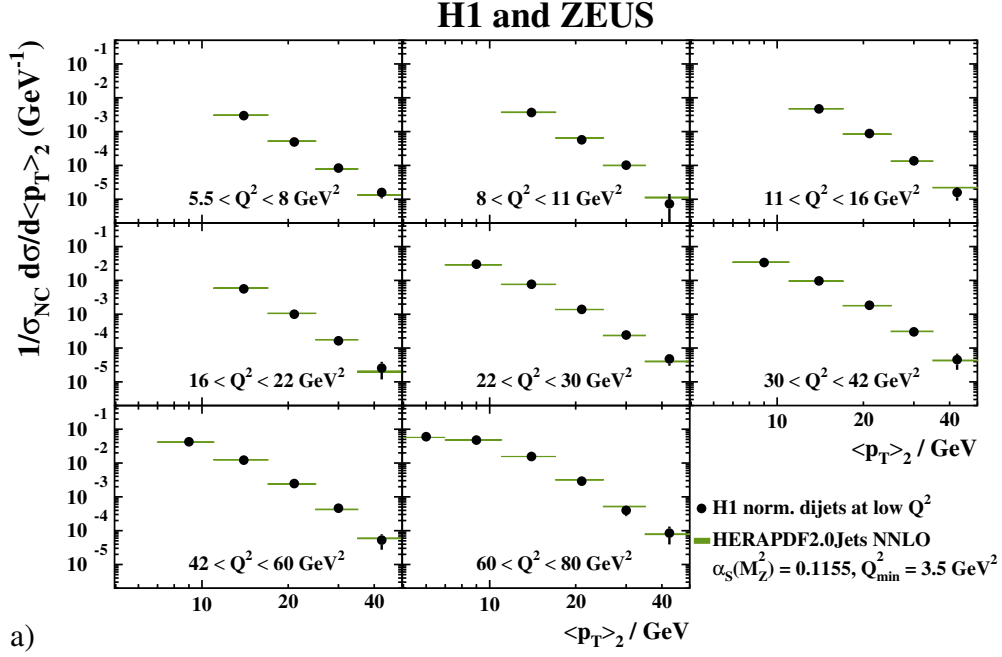


Figure 15: a) Differential dijet cross sections, $d\sigma/d\langle p_T \rangle_2$, normalised to NC inclusive cross sections, in bins of Q^2 between 5 and 80 GeV^2 as measured by H1. The variable $\langle p_T \rangle_2$ denotes the average p_T of the two jets. Also shown are predictions based on HERAPDF2.0Jets NNLO. The bands represent the total uncertainties on the predictions excluding scale uncertainties; the bands are mostly invisible. Only data used in the fit are shown. b) Measured cross sections divided by predictions based on HERAPDF2.0Jets NNLO.

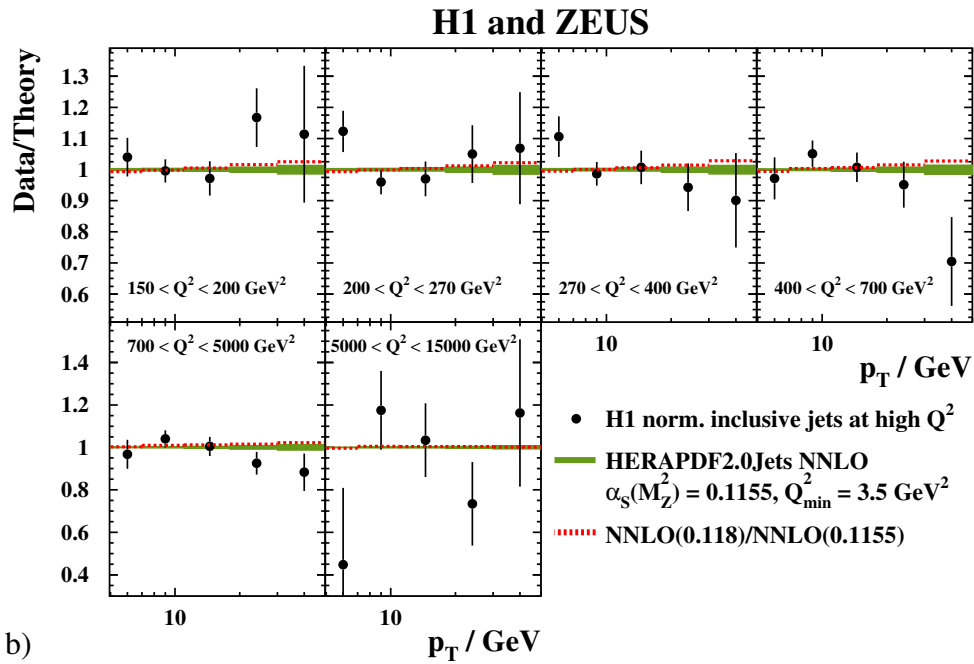
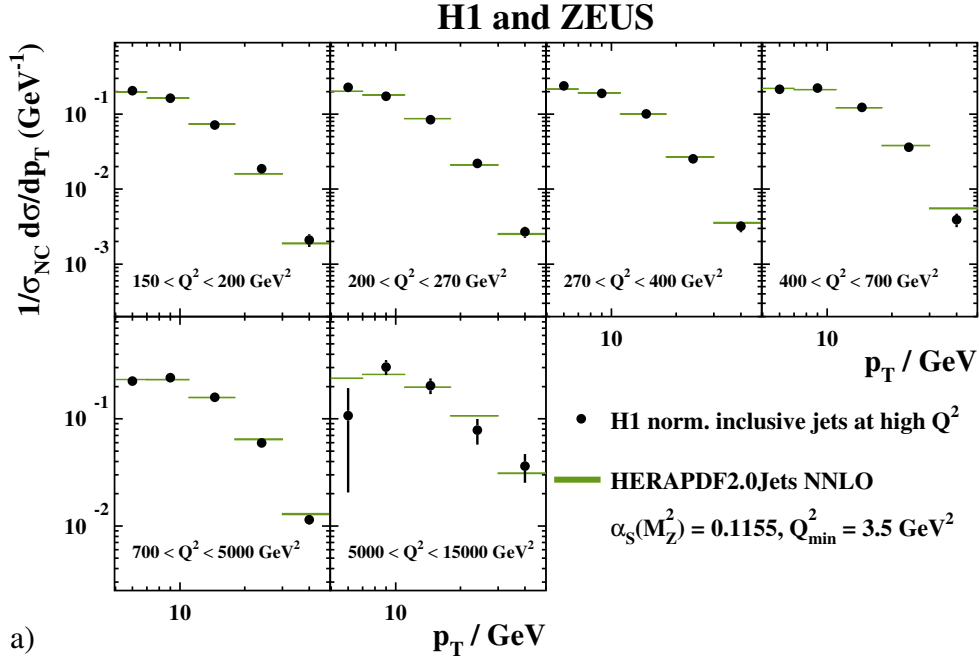


Figure 16: a) Differential jet cross sections, $d\sigma/dp_T$, normalised to NC inclusive cross sections, in bins of Q^2 between 150 and 15000 GeV^2 as measured by H1. Also shown are predictions based on HERAPDF2.0Jets NNLO. The bands represent the total uncertainties on the predictions excluding scale uncertainties; the bands are mostly invisible. Only data used in the fit are shown. b) Measured cross sections divided by predictions based on HERAPDF2.0Jets NNLO.

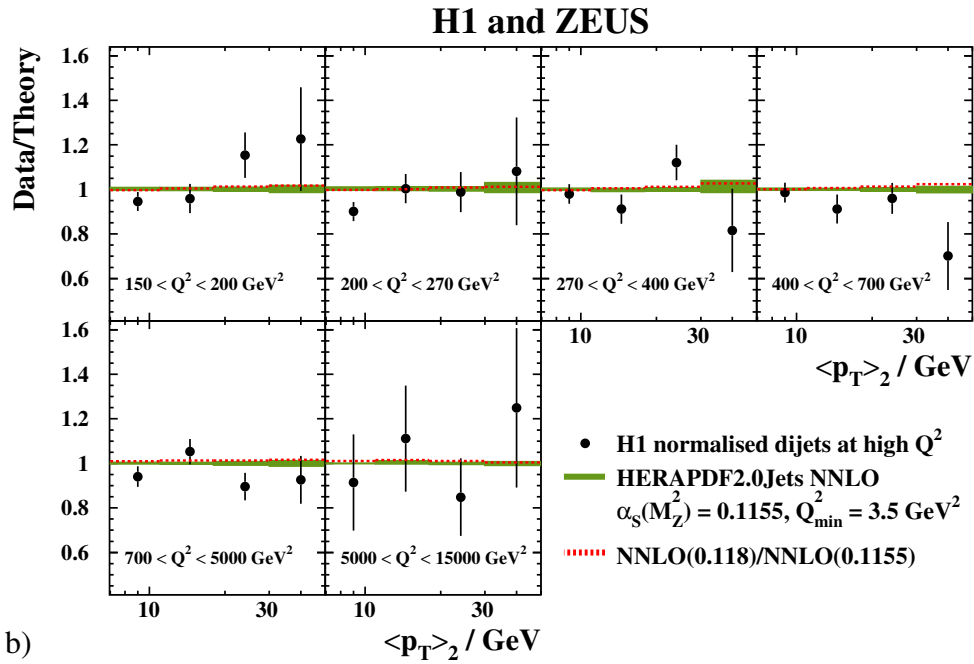
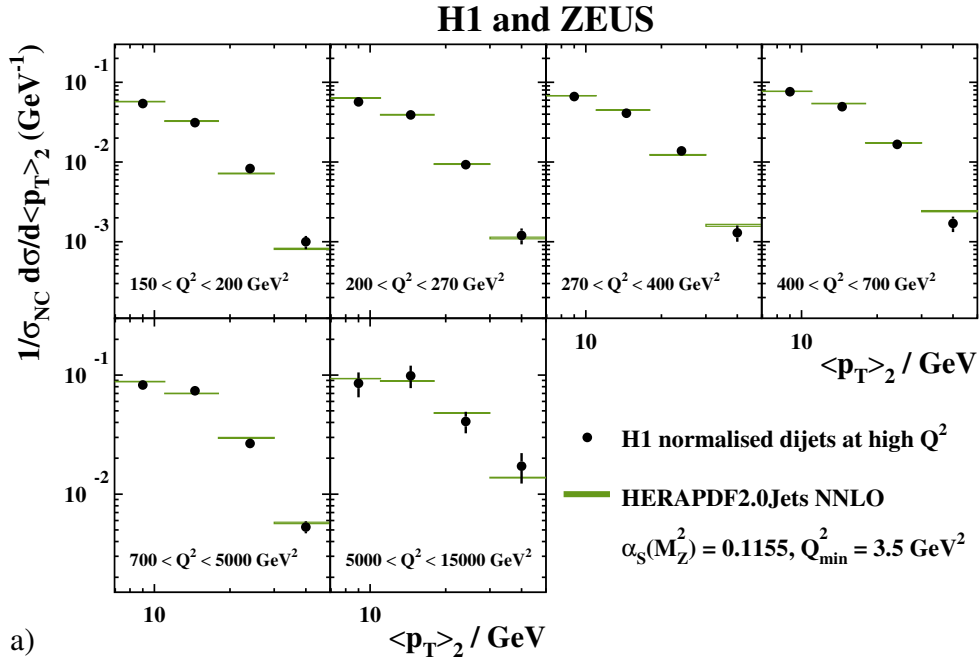


Figure 17: a) Differential dijet cross sections, $d\sigma/d\langle p_T \rangle_2$, normalised to NC inclusive cross sections, in bins of Q^2 between 150 and 15000 GeV^2 as measured by H1. The variable $\langle p_T \rangle_2$ denotes the average p_T of the two jets. Also shown are predictions based on HERAPDF2.0Jets NNLO. The bands represent the total uncertainties on the predictions excluding scale uncertainties; the bands are mostly invisible. Only data used in the fit are shown. b) Measured cross sections divided by predictions based on HERAPDF2.0Jets NNLO.

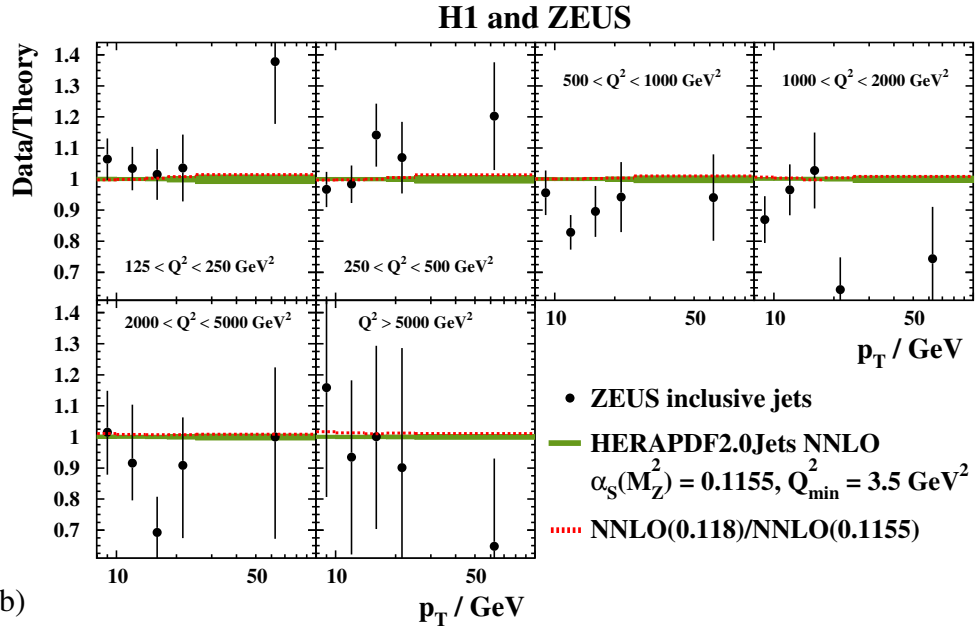
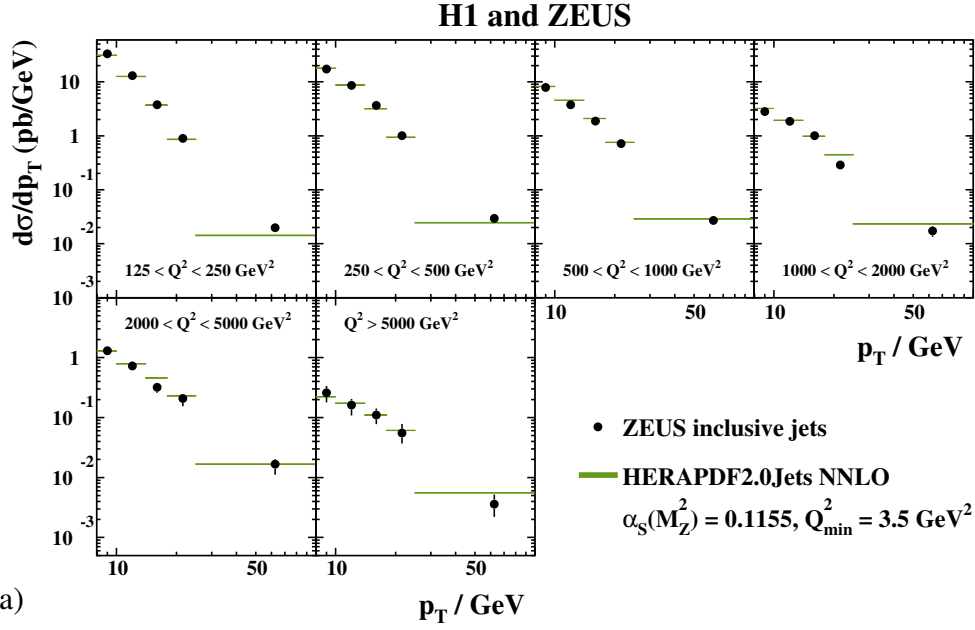


Figure 18: a) Differential jet cross sections, $d\sigma/dp_T$, in bins of Q^2 between 125 and 10000 GeV^2 as measured by ZEUS. Also shown are predictions based on HERAPDF2.0Jets NNLO. The bands represent the total uncertainty on the predictions excluding scale uncertainties; the bands are mostly invisible. Only data used in the fit are shown. b) Measured cross sections divided by predictions based on HERAPDF2.0Jets NNLO.

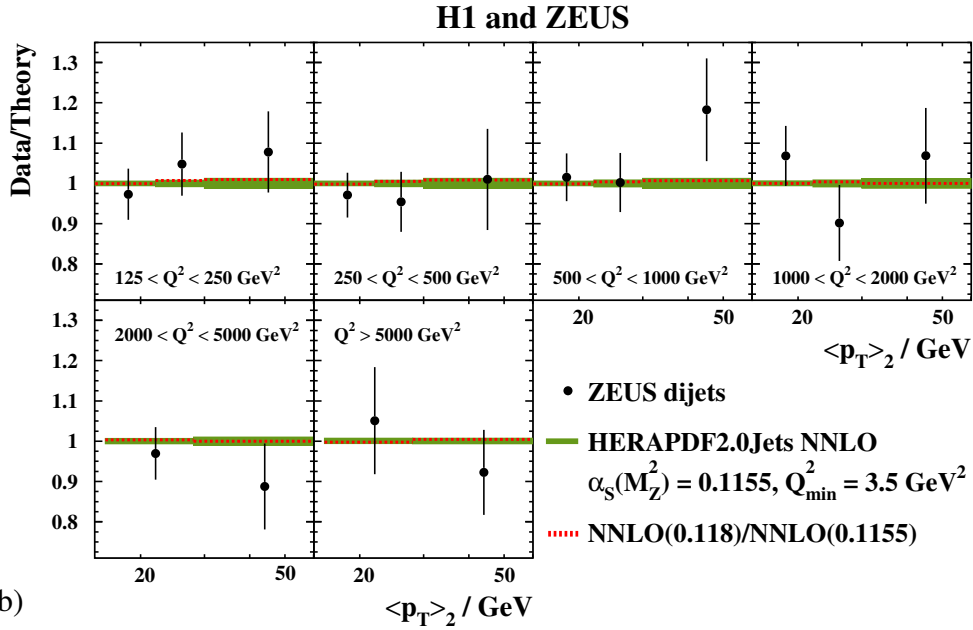
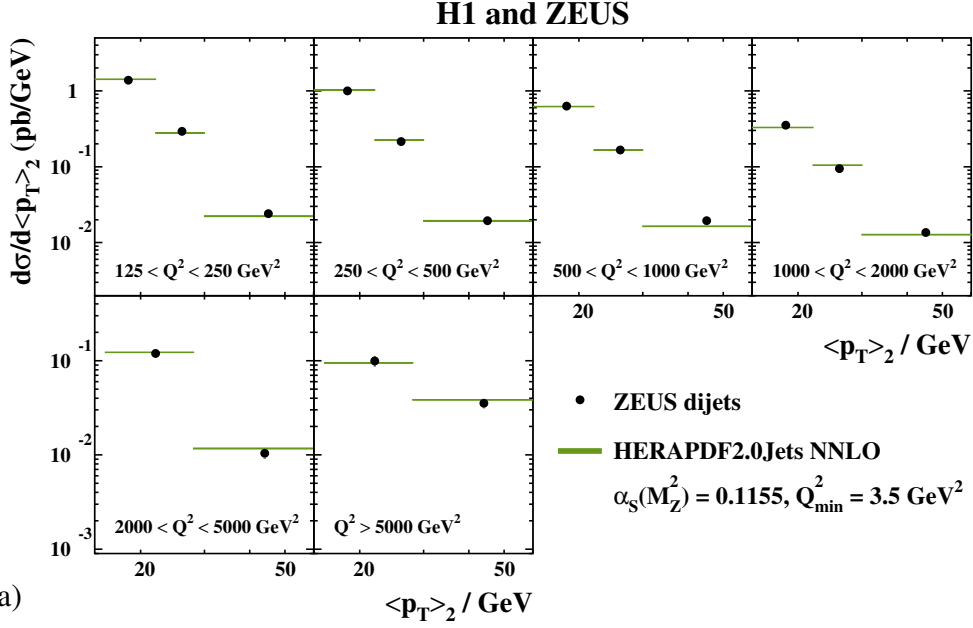


Figure 19: a) Differential dijet cross sections, $d\sigma/d\langle p_T \rangle_2$, in bins of Q^2 between 125 and 20000 GeV^2 as measured by ZEUS. The variable $\langle p_T \rangle_2$ denotes the average p_T of the two jets. Also shown are predictions based on HERAPDF2.0Jets NNLO. The bands represent the total uncertainty on the predictions excluding scale uncertainties; the bands are mostly invisible. Only data used in the fit are shown. b) Measured cross sections divided by predictions based on HERAPDF2.0Jets NNLO.

Appendix A:

PDF sets released

The following two sets of PDFs are released [41] and available on LHAPDF:

(<https://lhapdf.hepforge.org/pdfsets.html>).

- HERAPDF2.0Jets NNLO

- based on the combination of inclusive data from the H1 and ZEUS collaborations and selected data on jet production;
- with $Q_{\min}^2 = 3.5 \text{ GeV}^2$;
- using the RTOPT variable-flavour-number scheme;
 - * with fixed value of $\alpha_s(M_Z^2) = 0.01155$;
 - * with fixed value of $\alpha_s(M_Z^2) = 0.0118$;
- 14 eigenvector pairs give Hessian experimental (fit) uncertainties including hadronisation uncertainties;
- grids of 14 variations are released to describe the model and parameterisation uncertainties.

Appendix B:

Additional ratio plots on gluon PDF uncertainties

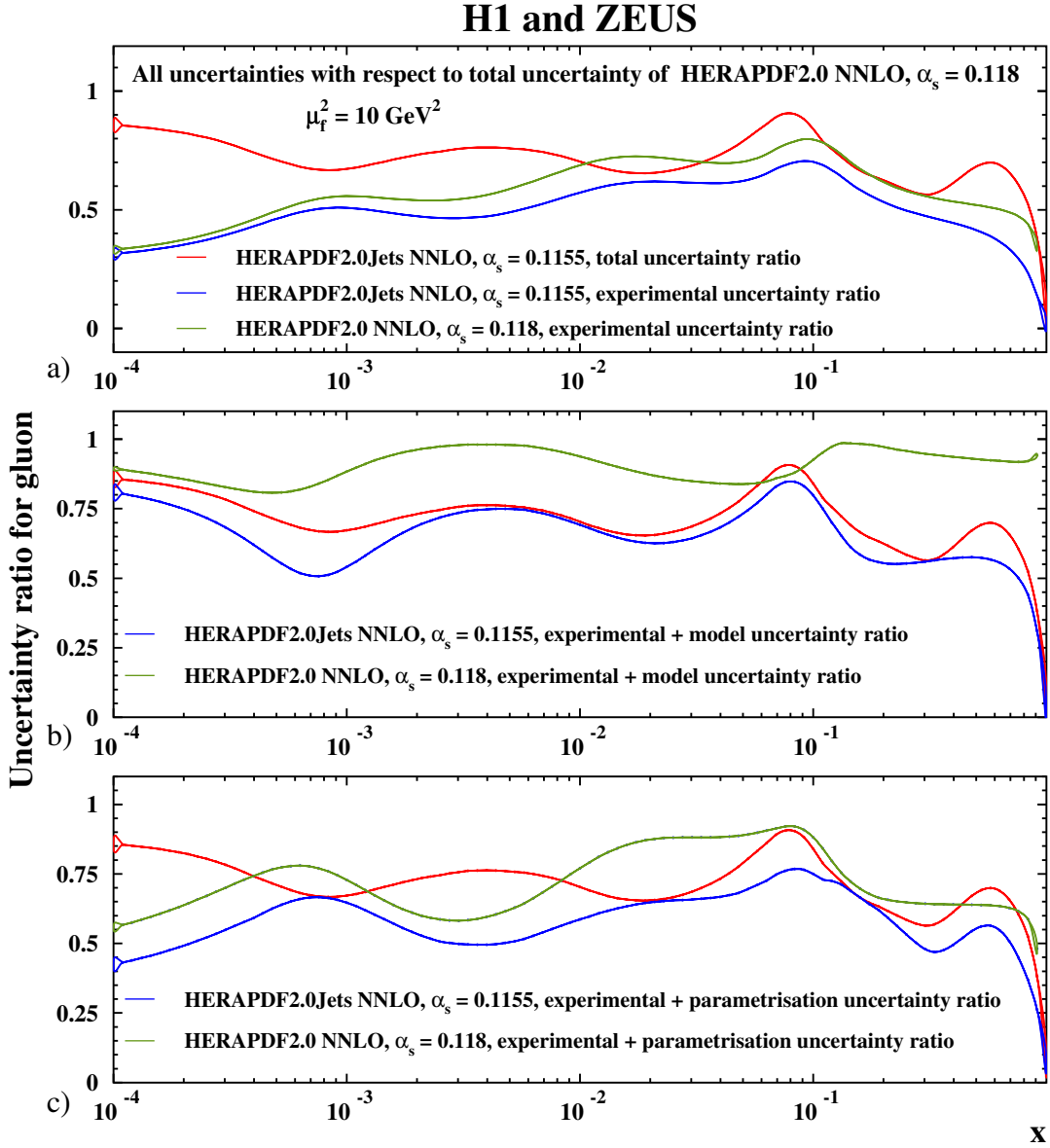


Figure 20: Ratios of uncertainties relative to the total uncertainties of HERAPDF2.0 NNLO $\alpha_s(M_Z^2) = 0.118$ for the total uncertainty of HERAPDF2.0Jets NNLO $\alpha_s(M_Z^2) = 0.1155$ and the a) experimental uncertainty of HERAPDF2.0Jets NNLO $\alpha_s(M_Z^2) = 0.1155$ as well as the experimental uncertainty of HERAPDF2.0 NNLO $\alpha_s(M_Z^2) = 0.118$, b) experimental plus model uncertainty of HERAPDF2.0Jets NNLO $\alpha_s(M_Z^2) = 0.1155$ as well as the experimental plus model uncertainty of HERAPDF2.0 NNLO $\alpha_s(M_Z^2) = 0.118$, c) experimental plus parameterisation uncertainty of HERAPDF2.0Jets NNLO $\alpha_s(M_Z^2) = 0.1155$ as well as the experimental plus parameterisation uncertainty of HERAPDF2.0 NNLO $\alpha_s(M_Z^2) = 0.118$, at the scale $\mu_f^2 = 10 \text{ GeV}^2$.

H1 and ZEUS

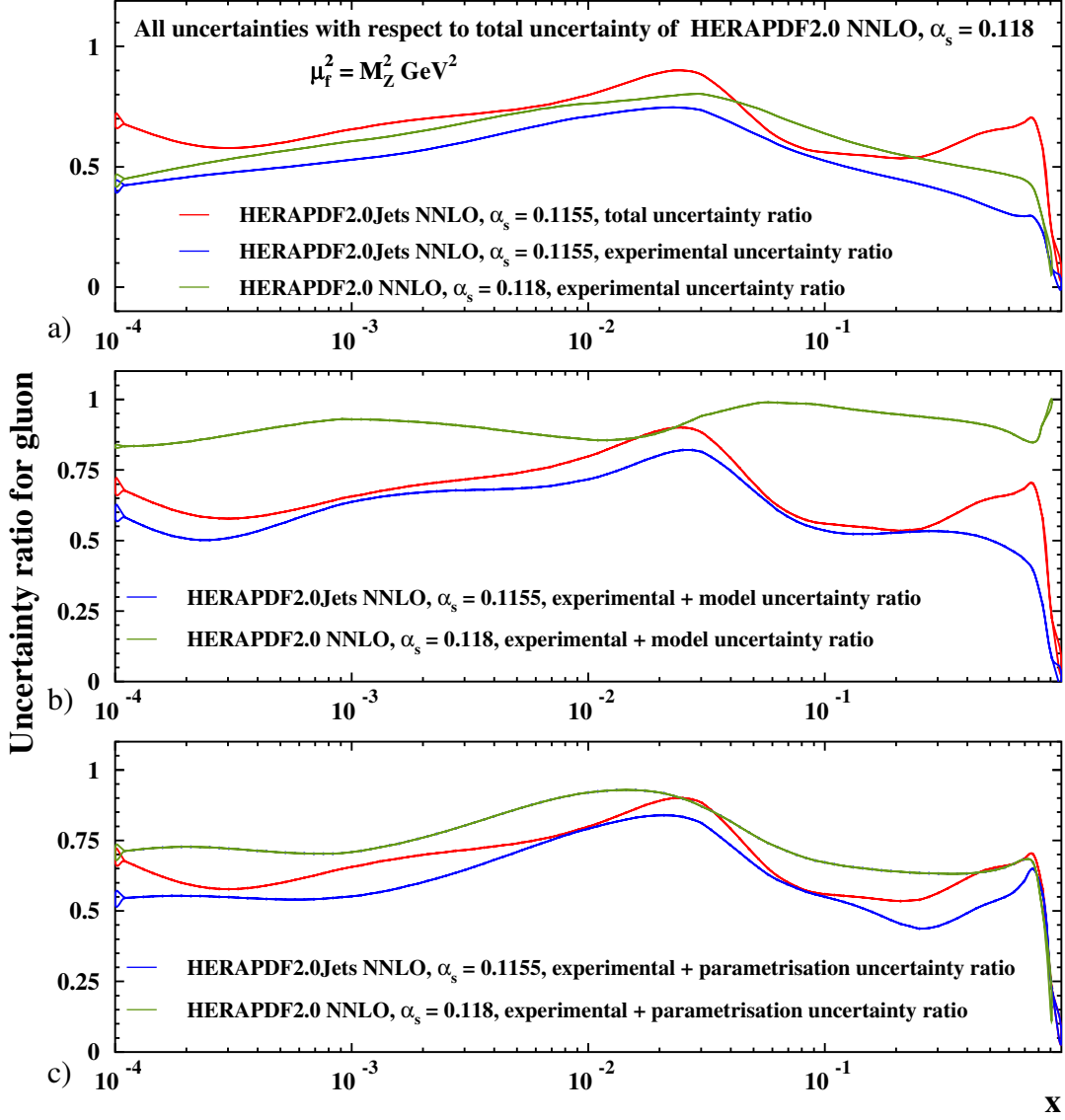


Figure 21: Ratios of uncertainties relative to the total uncertainties of HERAPDF2.0 NNLO $\alpha_s(M_Z^2) = 0.118$ for the total uncertainty of HERAPDF2.0Jets NNLO $\alpha_s(M_Z^2) = 0.1155$ and the a) experimental uncertainty of HERAPDF2.0Jets NNLO $\alpha_s(M_Z^2) = 0.1155$ as well as the experimental uncertainty of HERAPDF2.0 NNLO $\alpha_s(M_Z^2) = 0.118$, b) experimental plus model uncertainty of HERAPDF2.0Jets NNLO $\alpha_s(M_Z^2) = 0.1155$ as well as the experimental plus model uncertainty of HERAPDF2.0 NNLO $\alpha_s(M_Z^2) = 0.118$, c) experimental plus parameterisation uncertainty of HERAPDF2.0Jets NNLO $\alpha_s(M_Z^2) = 0.1155$ as well as the experimental plus parameterisation uncertainty of HERAPDF2.0 NNLO $\alpha_s(M_Z^2) = 0.118$, at the scale $\mu_f^2 = M_Z^2$.

H1 and ZEUS

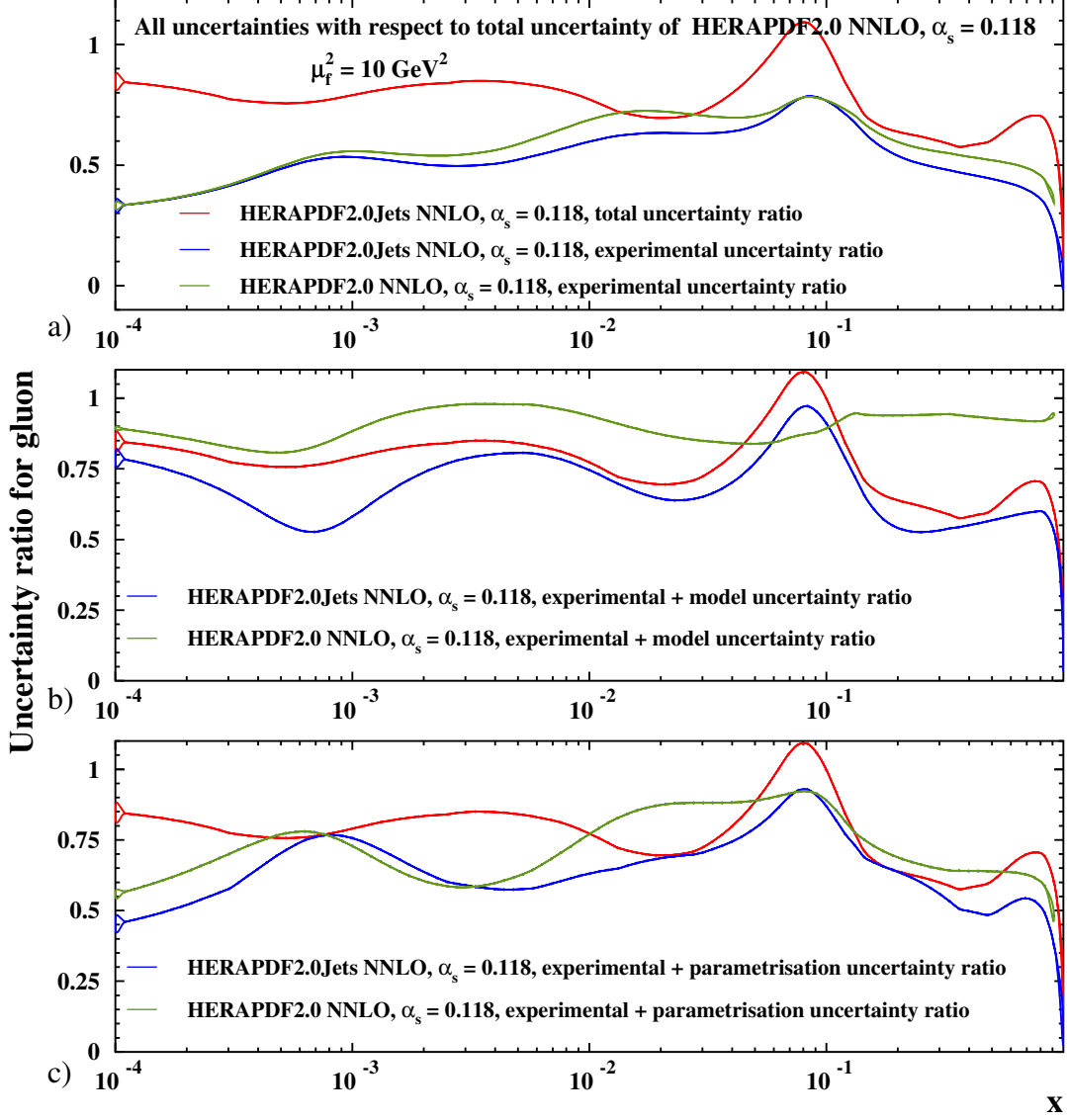


Figure 22: Ratios of uncertainties relative to the total uncertainties of HERAPDF2.0 NNLO $\alpha_s(M_Z^2) = 0.118$ for the total uncertainty of HERAPDF2.0Jets NNLO $\alpha_s(M_Z^2) = 0.118$ and the a) experimental uncertainty of HERAPDF2.0Jets NNLO $\alpha_s(M_Z^2) = 0.118$ as well as the experimental uncertainty of HERAPDF2.0 NNLO $\alpha_s(M_Z^2) = 0.118$, b) experimental plus model uncertainty of HERAPDF2.0Jets NNLO $\alpha_s(M_Z^2) = 0.118$ as well as the experimental plus model uncertainty of HERAPDF2.0 NNLO $\alpha_s(M_Z^2) = 0.118$, c) experimental plus parameterisation uncertainty of HERAPDF2.0Jets NNLO $\alpha_s(M_Z^2) = 0.118$ as well as the experimental plus parameterisation uncertainty of HERAPDF2.0 NNLO $\alpha_s(M_Z^2) = 0.118$, at the scale $\mu_f^2 = 10 \text{ GeV}^2$.

H1 and ZEUS

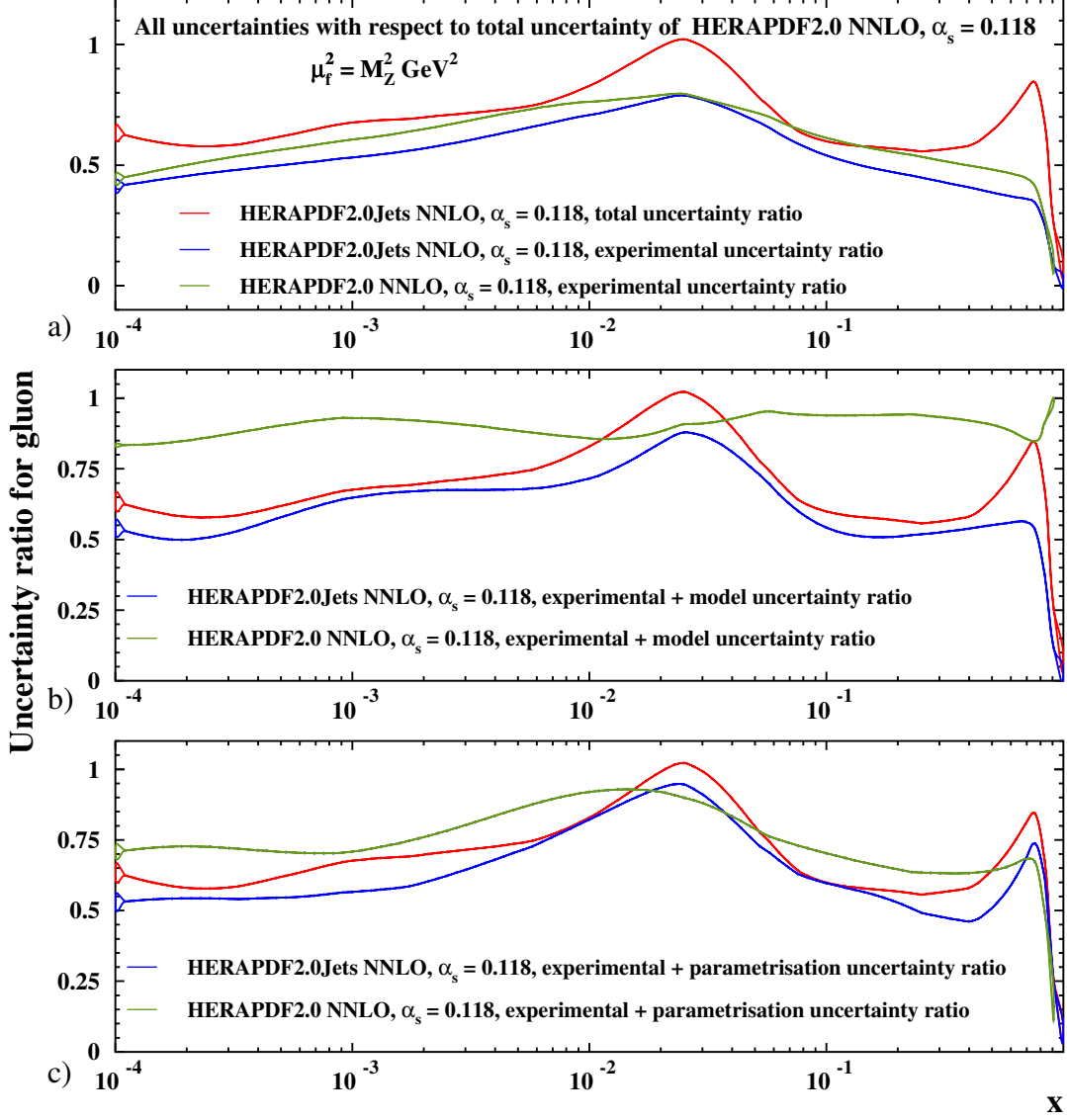


Figure 23: Ratios of uncertainties relative to the total uncertainties of HERAPDF2.0 NNLO $\alpha_s(M_Z^2) = 0.118$ for the total uncertainty of HERAPDF2.0Jets NNLO $\alpha_s(M_Z^2) = 0.118$ and the a) experimental uncertainty of HERAPDF2.0Jets NNLO $\alpha_s(M_Z^2) = 0.118$ as well as the experimental uncertainty of HERAPDF2.0 NNLO $\alpha_s(M_Z^2) = 0.118$, b) experimental plus model uncertainty of HERAPDF2.0Jets NNLO $\alpha_s(M_Z^2) = 0.118$ as well as the experimental plus model uncertainty of HERAPDF2.0 NNLO $\alpha_s(M_Z^2) = 0.118$, c) experimental plus parameterisation uncertainty of HERAPDF2.0Jets NNLO $\alpha_s(M_Z^2) = 0.118$ as well as the experimental plus parameterisation uncertainty of HERAPDF2.0 NNLO $\alpha_s(M_Z^2) = 0.118$, at the scale $\mu_f^2 = M_Z^2$.

Internal extra material:

Comparison of results on $\alpha_s(M_Z^2)$ determined at NLO and NNLO:

A more detailed comparison between the NLO and NNLO results must account for the following differences:

- the choice of scale was different;
- the NLO result did not include the recently published H1 low- Q^2 inclusive and dijet data [13];
- the NLO result did not include the newly published low p_T points from the H1 high- Q^2 inclusive data;
- the NNLO result does not include trijet data;
- the NNLO result does not include the low p_T points from the ZEUS dijet data;
- the NNLO analysis imposes a stronger kinematic cut $\mu > 10.0$ GeV;
- the treatment of hadronisation uncertainty differs.

All these changes with respect to the NLO analysis had to be made to create a consistent environment for a fit at NNLO. At the same time, an NLO fit cannot be done under exactly the same conditions as the NNLO fit, since the H1 low Q^2 data cannot be well fitted at NLO. However, an NLO and an NNLO fit can be done under the common conditions:

- choice of scale, $\mu_f^2 = \mu_r^2 = Q^2 + p_T^2$;
- exclusion of the H1 low- Q^2 inclusive and dijet data;
- exclusion of the low- p_T points from the H1 high- Q^2 inclusive jet data;
- exclusion of trijet data;
- exclusion of low- p_T points from the ZEUS dijet data;
- exclusion of data with $\mu < 10.0$ GeV;
- hadronisation uncertainties treated as correlated systematic uncertainties as done in the NNLO analysis.

In this case, the values obtained were $\alpha_s(M_Z^2) = 0.1186 \pm 0.0014(\text{exp})$ at NLO and $\alpha_s(M_Z^2) = 0.1144 \pm 0.0013(\text{exp})$ at NNLO. The new NLO value of $\alpha_s(M_Z^2)$ agrees with the published [2] value of 0.1183. The change of the NNLO result from the preferred value of 0.1156 is mostly due to the exclusion of the H1 low Q^2 data and the low- p_T points at high Q^2 .

Internal extra material:

More detailed information concerning the source of uncertainties at a scale of 10 GeV^2 : The green band represents HERAPDF2.0Jets NNLO $\alpha_s(M_Z^2)=0.1155$ as obtained for the old procedure, i.e. with double counting.

This shows that the improvement is mainly due to jet data.

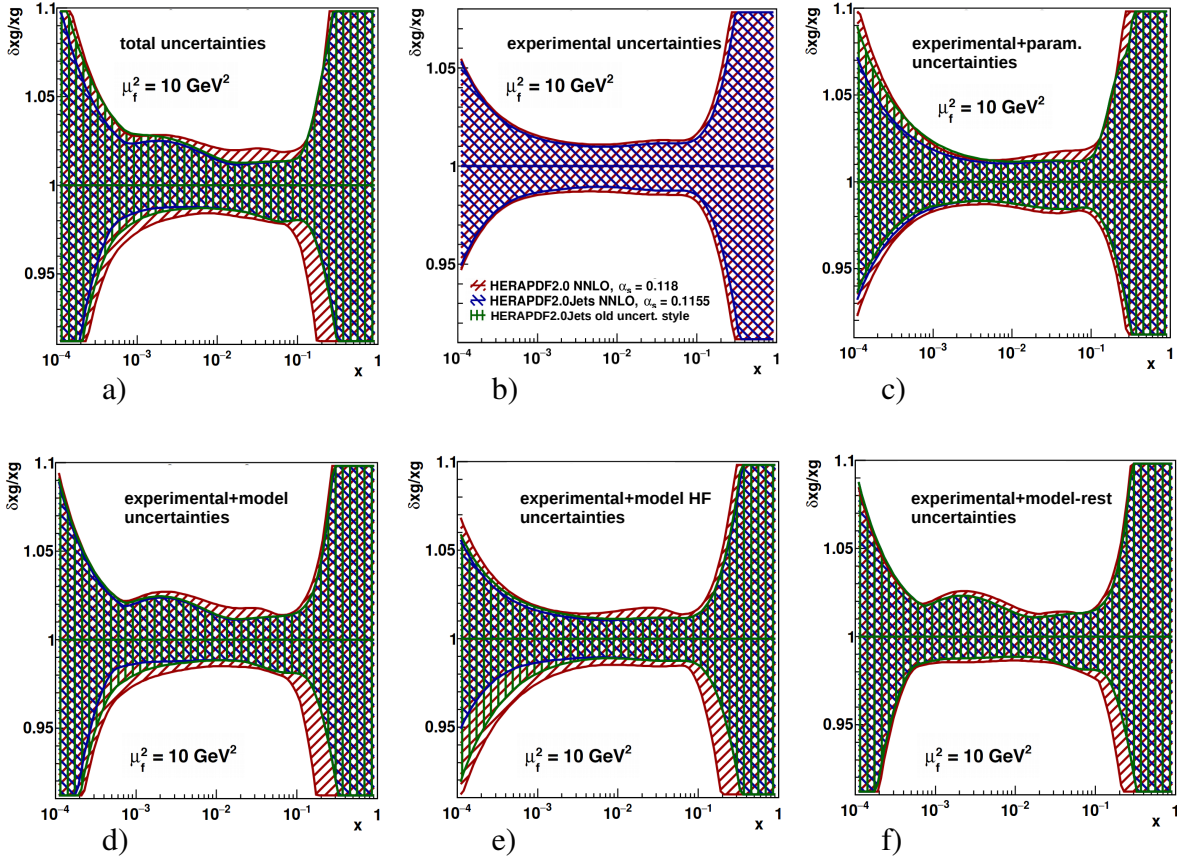


Figure 24: Comparison of the normalised uncertainties on the gluon PDFs of HERAPDF2.0Jets NNLO, HERAPDF2.0 NNLO and HERAPDF2.0Jets NNLO with old procedure on uncertainties for a) total, b) experimental, i.e. fit, c) experimental plus parameterisation, d) experimental plus model, e) experimental plus model due to heavy flavour f) experimental plus all model but heavy flavour uncertainties at the scale $\mu_f^2 = 10 \text{ GeV}^2$. The uncertainties on the three gluon distributions are shown as differently hatched bands.

Internal extra material:

507

508

509

510

511

More detailed information concerning the source of uncertainties at a scale of M_W^2 : The green band represents HERAPDF2.0Jets NNLO $\alpha_s(M_Z^2)=0.1155$ as obtained for the old procedure, i.e. with double counting.

This shows that the improvement is mainly due to jet data.

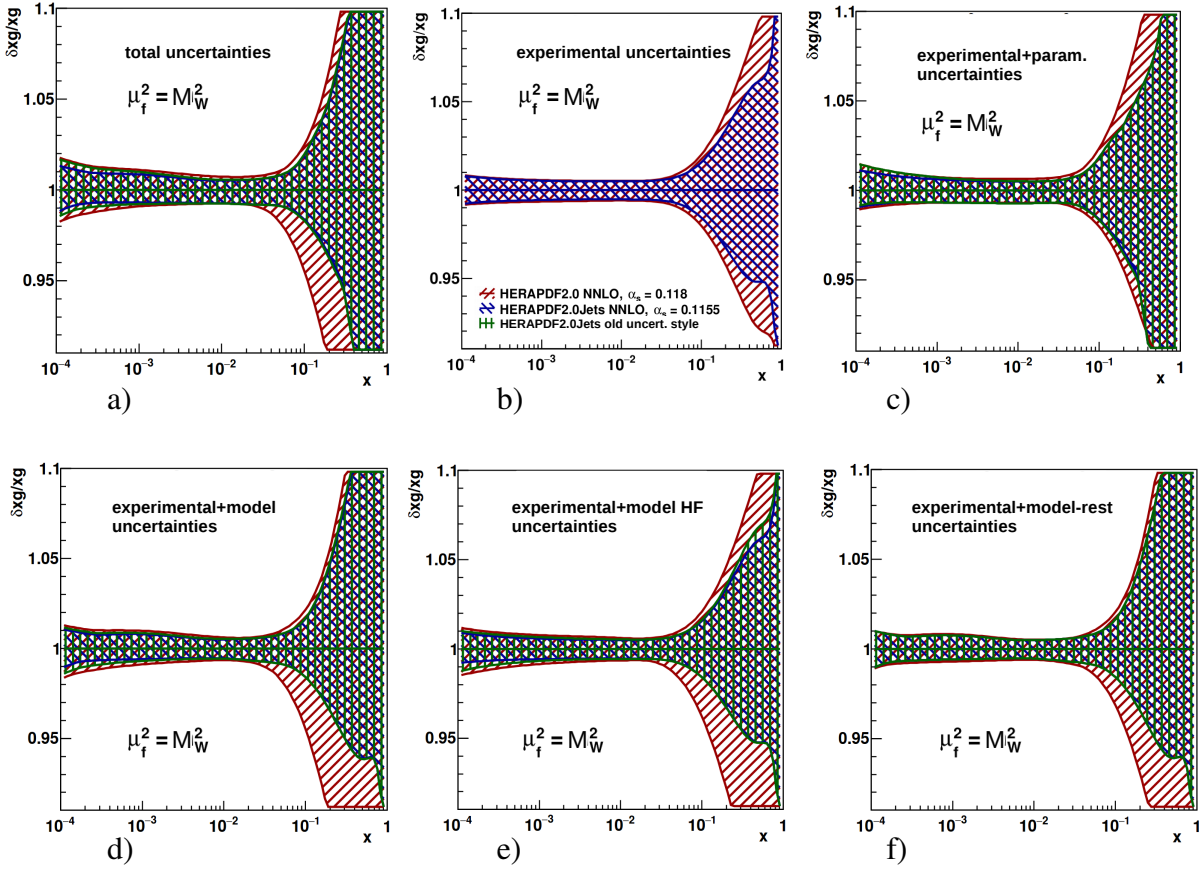


Figure 25: Comparison of the normalised uncertainties on the gluon PDFs of HERAPDF2.0Jets NNLO, HERAPDF2.0 NNLO and HERAPDF2.0Jets NNLO with old procedure on uncertainties for a) total, b) experimental, i.e. fit, c) experimental plus parameterisation, d) experimental plus model, e) experimental plus model due to heavy flavour f) experimental plus all model but heavy flavour uncertainties at the scale $\mu_f^2 = M_W^2$. The uncertainties on the three gluon distributions are shown as differently hatched bands.

Internal extra material:

```

513 Parameters as determined by the fits and their correlations
514 =====
515 PARAMETERS WITH UNCERTAINTIES:
516 =====
517 as free
518 =====
519 2 'Bg' -0.084608 0.071758
520 3 'Cg' 6.145485 0.553362
521 7 'Aprig' 0.148366 0.134036
522 8 'Bprig' -0.408486 0.062832
523 9 'Cprig' 25.000000 0.000000 fixed
524 12 'Buv' 0.782478 0.027706
525 13 'Cuv' 4.878155 0.083909
526 15 'Euv' 10.390885 1.352200
527 22 'Bdv' 0.983110 0.083080
528 23 'Cdv' 4.795152 0.383854
529 33 'CUBar' 7.123114 1.699099
530 34 'DUBar' 1.995344 2.431042
531 41 'ADbar' 0.262598 0.010781
532 42 'BDbar' -0.128810 0.004899
533 43 'CDbar' 9.094971 1.741850
534 101 'alphas' 0.115638 0.001142
535 as = 0.1155
536 =====
537 2 'Bg' -0.085574 0.039648
538 3 'Cg' 6.171545 0.496131
539 7 'Aprig' 0.147903 0.040820
540 8 'Bprig' -0.409380 0.028287
541 9 'Cprig' 25.000000 0.000000 fixed
542 12 'Buv' 0.781078 0.025867
543 13 'Cuv' 4.880050 0.080411
544 15 'Euv' 10.401539 1.289019
545 22 'Bdv' 0.983055 0.084572
546 23 'Cdv' 4.804735 0.380423
547 33 'CUBar' 7.125150 1.645404
548 34 'DUBar' 2.031948 2.222251
549 41 'ADbar' 0.262191 0.010036
550 42 'BDbar' -0.128934 0.004725
551 43 'CDbar' 9.161993 1.693978
552 as = 0.118
553 =====
554 2 'Bg' -0.070319 0.043016
555 3 'Cg' 5.670899 0.482567
556 7 'Aprig' 0.161572 0.043068
557 8 'Bprig' -0.391610 0.027755
558 9 'Cprig' 25.000000 0.000000 fixed
559 12 'Buv' 0.806334 0.028281
560 13 'Cuv' 4.844608 0.081284
561 15 'Euv' 10.242348 1.441602
562 22 'Bdv' 0.981522 0.092135
563 23 'Cdv' 4.622768 0.397334
564 33 'CUBar' 7.137838 1.347568
565 34 'DUBar' 1.458837 1.614989
566 41 'ADbar' 0.269978 0.010673
567 42 'BDbar' -0.126504 0.004831
568 43 'CDbar' 8.036277 1.509073
569 PARAMETER CORRELATION COEFFICIENTS
570 =====
571 as free
572 =====
573 NO. GLOBAL 2 3 7 8 12 13 15 22 23 33 34 41 42 43 101
574 2 0.99909 1.000 0.544-0.880-0.627 0.112-0.024-0.040 0.030-0.015 0.024 0.019-0.090-0.166-0.066 0.135
575 3 0.99544 0.544 1.000-0.294-0.077-0.034 0.078-0.036-0.095-0.060 0.141 0.242-0.452-0.503-0.226-0.386
576 7 0.99942 -0.880-0.294 1.000 0.914 0.101-0.067-0.115 0.033 0.028 0.010-0.001 0.025 0.028-0.026 0.002
577 8 0.99710 -0.627-0.077 0.914 1.000 0.251-0.130-0.230 0.094 0.057 0.010-0.028 0.038-0.009-0.062 0.093
578 12 0.99580 0.112-0.034 0.101 0.251 1.000-0.208-0.711 0.254 0.050 0.326 0.036 0.524 0.400 0.021 0.418
579 13 0.98055 -0.024 0.078-0.067-0.130-0.208 1.000 0.708-0.193-0.212 0.374 0.410-0.168-0.124-0.089-0.183
580 15 0.99428 -0.040-0.036-0.115-0.230-0.711 0.708 1.000-0.226-0.165 0.133 0.338-0.369-0.299-0.137-0.056
581 22 0.99034 0.030-0.095 0.033 0.094 0.254-0.193-0.226 1.000 0.892 0.370 0.287 0.266 0.228 0.591 0.020
582 23 0.98232 -0.015-0.060 0.028 0.057 0.050-0.212-0.165 0.892 1.000 0.151 0.114 0.154 0.147 0.553-0.197
583 33 0.99829 0.024 0.141 0.010 0.010 0.326 0.374 0.133 0.370 0.151 1.000 0.923-0.006-0.020 0.160 0.002
584 34 0.99812 0.019 0.242-0.001-0.028 0.036 0.410 0.338 0.287 0.114 0.923 1.000-0.253-0.252 0.228-0.108
585 41 0.97212 -0.090-0.452 0.025 0.038 0.524-0.168-0.369 0.266 0.154-0.006-0.253 1.000 0.950 0.168 0.330
586 42 0.97595 -0.166-0.503 0.028-0.009 0.400-0.124-0.299 0.228 0.147-0.020-0.252 0.950 1.000 0.188 0.220
587 43 0.98859 -0.066-0.226-0.026-0.062 0.021-0.089-0.137 0.591 0.553 0.160 0.228 0.168 0.188 1.000-0.291
588 101 0.99603 0.135-0.386 0.002 0.093 0.418-0.183-0.056 0.020-0.197 0.002-0.108 0.330 0.220-0.291 1.000
589 as = 0.1155
590 =====
591 NO. GLOBAL 2 3 7 8 12 13 15 22 23 33 34 41 42 43
592 2 0.99909 1.000 0.653-0.891-0.656 0.060 0.002-0.031 0.027 0.012 0.023 0.033-0.145-0.204-0.027
593 3 0.99467 0.653 1.000-0.325-0.056 0.160 0.023-0.053-0.078-0.144 0.171 0.230-0.374-0.465-0.372
594 7 0.99943 -0.891-0.325 1.000 0.920 0.109-0.063-0.112 0.034 0.029 0.014 0.004 0.028 0.032-0.025
595 8 0.99712 -0.656-0.056 0.920 1.000 0.231-0.111-0.221 0.092 0.076 0.012-0.013 0.010-0.027-0.035
596 12 0.99499 0.060 0.160 0.109 0.231 1.000-0.117-0.734 0.285 0.154 0.379 0.134 0.442 0.340 0.171
597 13 0.98052 0.002 0.023-0.063-0.111-0.117 1.000 0.713-0.154-0.239 0.418 0.433-0.118-0.092-0.132
598 15 0.99429 -0.031-0.053-0.112-0.221-0.734 0.713 1.000-0.203-0.171 0.161 0.344-0.373-0.296-0.148
599 22 0.99053 0.027-0.078 0.034 0.092 0.285-0.154-0.203 1.000 0.910 0.404 0.331 0.265 0.220 0.625
600 23 0.98154 0.012-0.144 0.029 0.076 0.154-0.239-0.171 0.910 1.000 0.169 0.115 0.233 0.196 0.530
601 33 0.99858 0.023 0.171 0.014 0.012 0.379 0.418 0.161 0.404 0.169 1.000 0.940-0.017-0.033 0.192
602 34 0.99841 0.033 0.230 0.004-0.013 0.134 0.433 0.344 0.331 0.115 0.940 1.000-0.223-0.229 0.228
603 41 0.96869 -0.145-0.374 0.028 0.010 0.442-0.118-0.373 0.265 0.233-0.017-0.223 1.000 0.953 0.287
604 42 0.97473 -0.204-0.465 0.032-0.027 0.340-0.092-0.296 0.220 0.196-0.033-0.229 0.953 1.000 0.264
605 43 0.98749 -0.027-0.372-0.025-0.035 0.171-0.132-0.148 0.625 0.530 0.192 0.228 0.287 0.264 1.000

```

```

606 as = 0.118
607 =====
608 NO. GLOBAL 2 3 7 8 12 13 15 22 23 33 34 41 42 43
609 2 0.99830 1.000 0.584-0.794-0.507 0.052-0.002-0.029-0.005-0.017 0.025 0.045-0.188-0.238-0.067
610 3 0.99467 0.584 1.000-0.086 0.184 0.146-0.004-0.071-0.148-0.192 0.160 0.233-0.432-0.517-0.453
611 7 0.99906 -0.794-0.086 1.000 0.917 0.190-0.095-0.183 0.071 0.059 0.029 0.015-0.019-0.048-0.030
612 8 0.99645 -0.507 0.184 0.917 1.000 0.308-0.142-0.288 0.115 0.094 0.033 0.008-0.065-0.131-0.053
613 12 0.99521 0.052 0.146 0.190 0.308 1.000-0.176-0.777 0.302 0.184 0.381 0.166 0.429 0.321 0.216
614 13 0.98045 -0.002-0.004-0.095-0.142-0.176 1.000 0.712-0.219-0.278 0.360 0.389-0.112-0.079-0.150
615 15 0.99461 -0.029-0.071-0.183-0.288-0.777 0.712 1.000-0.258-0.208 0.089 0.264-0.354-0.270-0.188
616 22 0.99185 -0.005-0.148 0.071 0.115 0.302-0.219-0.258 1.000 0.920 0.351 0.291 0.287 0.238 0.666
617 23 0.98399 -0.017-0.192 0.059 0.094 0.184-0.278-0.208 0.920 1.000 0.159 0.107 0.248 0.208 0.556
618 33 0.99867 0.025 0.160 0.029 0.033 0.381 0.360 0.089 0.351 0.159 1.000 0.948 0.010-0.006 0.135
619 34 0.99849 0.045 0.233 0.015 0.008 0.166 0.389 0.264 0.291 0.107 0.948 1.000-0.178-0.186 0.157
620 41 0.96829 -0.188-0.432-0.019-0.065 0.429-0.112-0.354 0.287 0.248 0.010-0.178 1.000 0.953 0.337
621 42 0.97500 -0.238-0.517-0.048-0.131 0.321-0.079-0.270 0.238 0.208-0.006-0.186 0.953 1.000 0.312
622 43 0.99021 -0.067-0.453-0.030-0.053 0.216-0.150-0.188 0.666 0.556 0.135 0.157 0.337 0.312 1.000

```